SAHC

Ductile connection characterization regarding seismic retrofitting of masonry buildings.

Tristan Hamilton Carles

Portugal | 2012

ADVANCED MASTERS IN STRUCTURAL ANALYSIS
OF MONUMENTS AND HISTORICAL CONSTRUCTIONS

Master's Thesis

Tristan Hamilton Carles

Ductile connection characterization regarding seismic retrofitting of masonry buildings.

University of Minho

Czech Technical University in Prague

Education and Culture

Erasmus Mundus

ADVANCED MASTERS IN STRUCTURAL ANALYSIS
OF MONUMENTS AND HISTORICAL CONSTRUCTIONS

Master's Thesis

Tristan Hamilton Carles

Ductile connection characterization regarding seismic retrofitting of masonry buildings.

This Masters Course has been funded with support from the European Commission. This publication reflects the views only of the author, and the Commission cannot be held responsible for any use which may be made of the information contained therein.

Portugal | 2012

DECLARATION

Name: Tristan Hamilton Carles

Email: tristan.carles@gmail.com

Title of the Msc Dissertation: Ductile connection characterization regarding seismic retrofitting of masonry buildings

Supervisor(s): Professor Luis Ramos

Year: 2012

I hereby declare that all information in this document has been obtained and presented in accordance with academic rules and ethical conduct. I also declare that, as required by these rules and conduct, I have fully cited and referenced all material and results that are not original to this work.

I hereby declare that the MSc Consortium responsible for the Advanced Masters in Structural Analysis of Monuments and Historical Constructions is allowed to store and make available electronically the present MSc Dissertation.

University: Universidade do Minho

Date: 16 July 2012

Signature:

_____

A cette alchimie égarée entre amour, amitié, et caféine ...

ACKNOWLEDGEMENTS

My first acknowledgments will go without any hesitation to my supervisor Professor Luis Ramos for his support and guidance throughout this thesis. This work would not have been accomplished on time, with this content, without his timely advise and suggestions. Moreover, his encouragement and patience were highly appreciated.

I would also like to thank the financial support provided by the SACH consortium without which I would have never been able to participate in this wonderful experience of the Erasmus Mundus Masters.

Many thanks as well to the PhD student Susana Moreira who was a huge help during the experimental campaign making the tests possible, along with her support and useful suggestions.

I could not mention the experiments carried out without expressing my gratitude to Senior Matos, a friendly technician from the structural laboratory from the University of Minho. It is more than likely that the experimental campaign would not have led to any valuable results without his help and support.

I would like to acknowledge Ana Fonseca and Alexandra Kurfurstova for their answers to many of my questions and the tremendous work they accomplished in order to make this master course so well organized.

My special thanks to my classmates who made this year in Prague and Minho unforgettable and so very special.

Last but not least, my heartfelt thanks to my family for supporting and encouraging me during all these years studying so far from home. Their love and trust was received as a force to go always a step further.

ABSTRACT

Anthropological reasons apart, earthquakes are one of the most devastating causes of damage to monuments and historical constructions, and, as a consequence, lead to significant cultural, human, and economical losses. Protection of such structures against seismic excitations is thus an important factor regarding life safety and the conservation of our historical heritage.

Efficient connections between structural elements can highly reduce the seismic vulnerability of masonry buildings by enhancing the out of plane behaviour of the walls regarding lateral loads which are presented as the principal cause of failure in this type of structure.

In spite of the importance of structural connections regarding the global behaviour of historical constructions under seismic actions, research in this field is almost nonexistent and needs to be developed.

The objective of this thesis is to study the seismic response to a ductile connection used to connect tie-rods to masonry walls in the scope of seismic retrofitting of historical constructions and to analyse its behaviour in comparison to the behaviour of the other structural elements.

In seismic vulnerability assessment, numerical models are of great importance and providing characterizations of such connections would be of considerable interest to architects and engineers in order to more accurately design a seismic retrofit and thus be able to predict and avoid expected damage.

Using a preliminary numerical model as a bench mark, the prototype was tested under monotonic and cyclic loading in order to reproduce similar excitations encountered during an earthquake. Based on the experimental campaign, a numerical model was developed and calibrated using the FE method. The comparison between the updated model and the experimental results helped to understand the fact that to a greater extent than the plasticization of the material, the parameter dissipating energy during the cycles is the friction between the plate and the walls.

It was concluded that this innovative ductile connexion was not as effective as had been expected in terms of seismic behaviour on account of the large residual displacements observed after a cyclic loading. Therefore, an alternative solution is proposed as well as implementation recommendations.

Key words: Seismic retrofitting, Innovative connection, ductile anchor plate, steel tie, experimental analysis, numerical modelling.

RESUMO

Titulo: Caracterização de ligações dúcteis para reforço sísmico de estruturas de alvenaria

À parte das razões antropológicas, os sismos são uma das maiores causas de dano para os monumentos e construções históricas, levando a perdas significativas a nível económico, cultural e humano. A proteção deste tipo de estruturas face às ações sísmicas é um fator relevante para a segurança e conservação do património histórico.

A eficiência das ligações entre elementos estruturais pode amplamente reduzir a vulnerabilidade sísmica dos edifícios, através do melhoramento do comportamento para fora do plano das paredes de alvenaria, atenuando o principal modo de colapso destas estruturas quando sujeitas a ações horizontais.

Apesar da importância das ligações estruturais no contexto do comportamento global de construções históricas quando sujeitas a ações sísmicas, a investigação neste campo é escassa e necessita de ser claramente ampliada.

Para avaliação da vulnerabilidade sísmica a utilização de modelos numéricos é de grande importância. A caracterização e a definição do comportamento real a nível numérico são fundamentais para os projetistas, uma vez que estes necessitam de uma previsão adequada do comportamento das ligações e da sua influência no comportamento estrutural para evitar o dano.

O objetivo da presente dissertação é estudar a resposta de uma ligação dúctil (placa de ancoragem) utilizada para ligar tirantes a paredes de alvenaria, passível de ser utilizada no reforço sísmico de construções históricas, analisando o seu comportamento sísmico de uma forma integrada com o comportamento dos restantes elementos estruturais.

Partindo de um modelo numérico preliminar desenvolvido de raiz e usando-o como um ponto de referência, foram realizados ensaios monotónicos e cíclicos para a caracterização estrutural da ligação. Com base na campanha experimental, o modelo numérico foi calibrado. A comparação entre o modelo calibrado e os resultados experimentais ajudou a compreender a resposta estrutural da ligação, o mecanismo de colapso, a dissipação de energia durante os ciclos, entre outros.

Com a presente dissertação concluiu-se que a ligação dúctil estudada, em termos de comportamento sísmico, não teve a resposta estrutural esperada, uma vez que foram observadas das grandes deformações residuais, tendo sido apresentada uma solução alternativa, bem como recomendações para a sua implementação.

Palavras Chave: ligações, placas de ancoragem dúcteis, tirantes, análise experimental, análise numérica.

RESUMÉ

Titre : Etude d'une connexion flexible dans le cadre d'un renforcement séismique de bâtiments en maçonnerie.

Sans parler des raisons anthropologiques, les tremblements de terre sont une des causes les plus dévastatrices des dégâts occasionnés aux monuments et constructions historiques, ce qui engendre en conséquence d'importantes pertes en termes humain, culturel et économique. Protéger ces structures est, par conséquent, un facteur de grande importance vis-à-vis de la sécurité de la population et de la conservation de notre patrimoine culturel.

La vulnérabilité séismique des bâtiments en maçonnerie peut être réduite de manière conséquente en connectant efficacement les différents éléments structuraux ce qui a pour conséquence d'améliorer le comportement des murs vis-à-vis des déformations hors du plan.

Malgré l'importance de ces connexions au regard du comportement global des constructions historiques soumises à une action séismique, la recherche dans ce domaine est presque inexistante et nécessite d'être développé.

L'objectif de cette thèse est d'étudier la réponse séismique d'une connexion flexible, utilisé pour ancrer les tirants aux murs de maçonnerie, dans le but d'un renforcement séismique de bâtiments historique et de comparer son comportement vis-à-vis des autres éléments structuraux.

Les model numériques sont d'une grande importance au regard des études de vulnérabilité séismique et la définition des caractéristiques de telles connexions pourrait être d'une grande contribution pour les architectes et ingénieur afin d'être plus proche de la réalité dans leur démarche de conception et en conséquence prévoir et éviter de nombreux dégâts.

En se servant d'un modèle numérique préliminaire comme repère, le prototype a été testé sous un chargement cyclique afin de reproduire une excitation similaire à celle ressentie lors d'un tremblement de terre. Basé sur cette campagne expérimentale, le modèle numérique a ensuite été développé et calibré utilisant la méthode des EF. La comparaison entre le modèle final et les tests menés a permis de démontrer qu'à plus grande échelle que la plastification de l'acier, le paramètre permettant de dissiper de l'énergie était la friction entre l'assiette ductile et le mur.

Pour conclure, il est démontré que cette connexion innovatrice ne fonctionne pas aussi bien que prévu au regard de son comportement séismique du fait des grandes déformations résiduelles observées après chaque cycle de charge.

Mots clés : Renforcement séismique, ancrage flexible, tirant, analyse expérimental, modélisation numérique.

TABLE OF CONTENTS

LIST OF FIGURES

LIST OF TABLES

CHAPTER 1: INTRODUCTION

1 SEISMIC VULNERABILITY

1.1 Related notions and definitions

Seismic vulnerability is highly related to seismic risk. The seismic risk is defined as the expected amount of damage for a given place, sustained by objects, buildings and people as a consequence of a seismic event [1]. It can be divided into three factors: hazard, exposure and vulnerability. In [2], the authors relate these factors through the equation 1

$$\text{risk} = \text{hazard} \times \text{vulnerability} \times \text{exposure} \quad (1)$$

We define the seismic hazard for a given area as the ground motion expected within a given time period. More precisely, the seismic hazard is the probability of occurrence of this ground shaking. The most common parameter to express the excitation is the maximum peak of the ground horizontal acceleration. It is the first step in the evaluation of seismic risk.

The calculation for seismic hazard involves different aspects such as the regional geology and seismology or mathematical expressions. The final result provides a probability of exceeding a value (usually the peak ground acceleration) within a time interval as shown on Figure 1.

The exposure corresponds to the estimation of the quantity, quality and value of all casualtie and injury to individuals, economic cost related to repair works or loss of cultural heritage associated to the seismic action. This notion is therefore closely connected to the distribution, structure and socio-economic system of a whole community [1].

The last factor that appears in the seismic risk formulation is the seismic vulnerability which is linked to the scope of this study.

A qualitative definition of this concept is presented in [3] as “the proneness of some category of elements at risk to undergo adverse effects inflicted by potential earthquakes”. Applied to a building, the seismic vulnerability corresponds to its behaviour described via a cause-effect law, where the cause is the earthquake and the effect is the damage [1]. This concept will be developed in the following subparts.

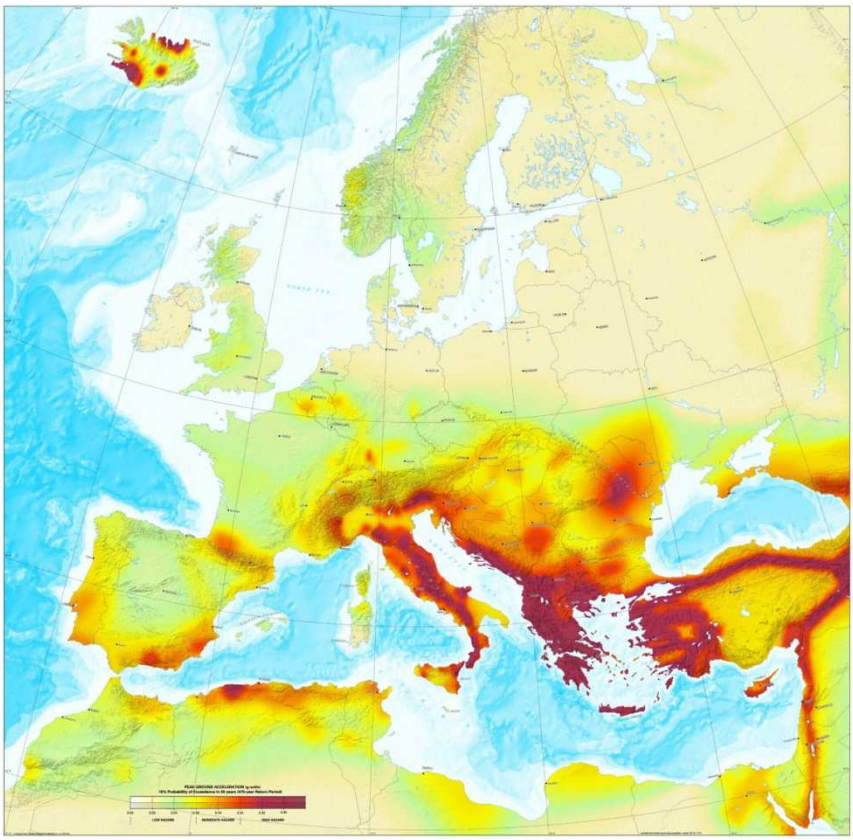

Figure 1 Seismic hazard map of Europe for 2003 (Source: European seismological Commission)

1.2 Assessment methodology

Seismic vulnerability assessment aims to characterize the seismic demand of the earthquake on the building which means the assessment needs to be carried out for a particular characterization of the ground motion. Traditionally, the analyzed parameter was related to macroseismic intensity or peak ground acceleration (PGA), whereas nowadays the vulnerability of a building is more commonly linked to response spectra obtained from past ground motions.

Figure 2 summarizes the various methods for vulnerability assessment that have been proposed in the past for use in loss evaluation. According to [4], we can divide them into two main categories: empirical or analytical, which can both be used in the hybrid method.

Empirical methods, which can also be called “damage-motion relationships”, are based on the damage observed after earthquakes and could be separated into two main types:

- Damage probability matrices (DPM), which express a conditional probability of obtaining a damage level (j) due to a ground motion of intensity (i) in a discrete form; this traditional assessment method is represented with a bold path on Figure 2.
- Vulnerability functions, which express the probability of exceeding a given damage state, given a function of the earthquake intensity, by means of continuous functions.

On the other hand, analytical methods relate post-earthquake damage statistics to limit-state mechanical properties of the buildings and appear to present more detailed and clearer vulnerability assessment algorithms with direct physical meaning. These characteristics, which are a real disadvantage for empirical methods, are very useful in studies such as parametric studies with retrofitting purposes for example. The development of these analytical methods is mainly due to the emergence of seismic hazard expressed in terms of response spectra obtained from ground motions.

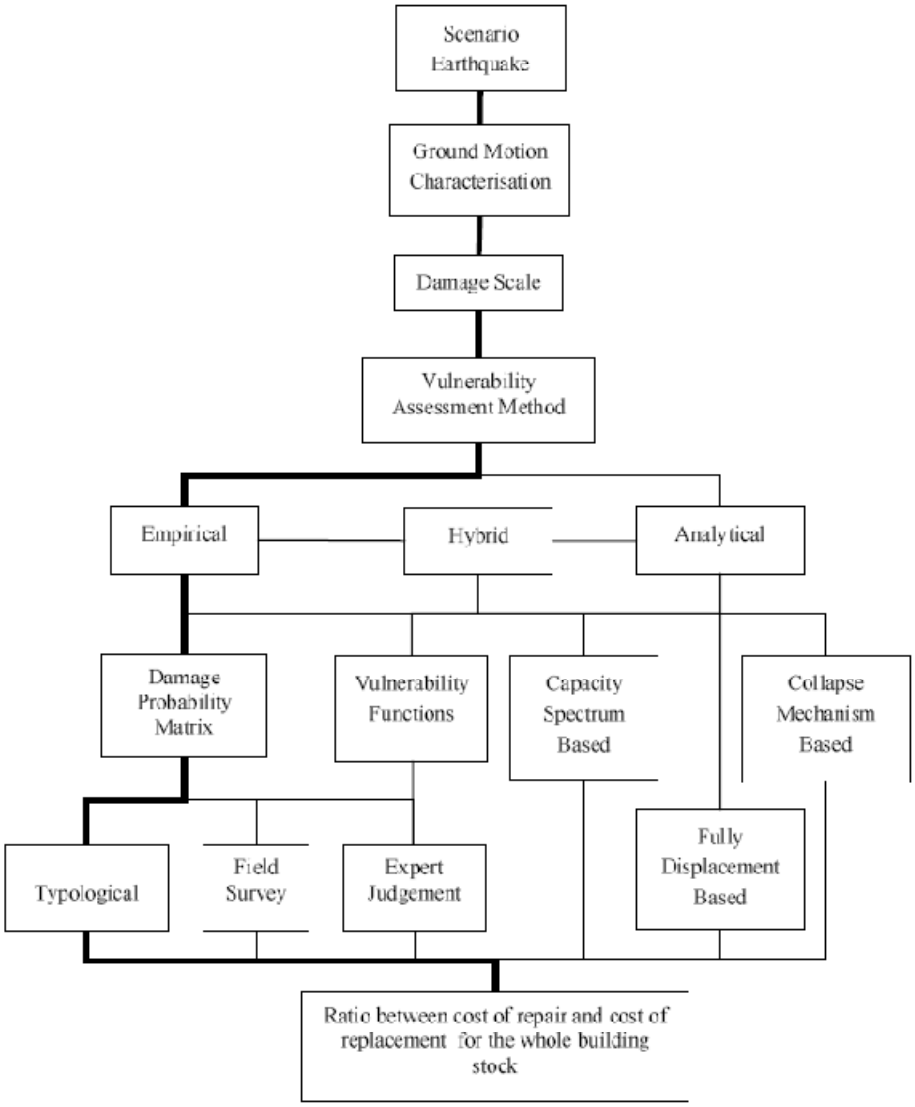

Figure 2 The components of seismic risk assessment and choices for the vulnerability assessment procedure [4]

In this way, it is of great importance to understand how a structure behaves under seismic actions not only in its present state but also with the influence of retrofitting initiatives. The more the behaviour is understood the more the model will be accurate and then the more the risk and loss assessment will be explicit and relevant.

2 DESCRIPTION OF THE TOPIC

This dissertation deals with masonry and timber connections between horizontal diaphragms (floors, roofs) and vertical structural elements (walls) in the scope of a seismic retrofitting of historical constructions.

It focuses on a specific type of innovative connection, more particularly a ductile anchor plate for steel tie rods or timber beams anchorage which is designed to dissipate energy in case of a hypothetical seismic action.

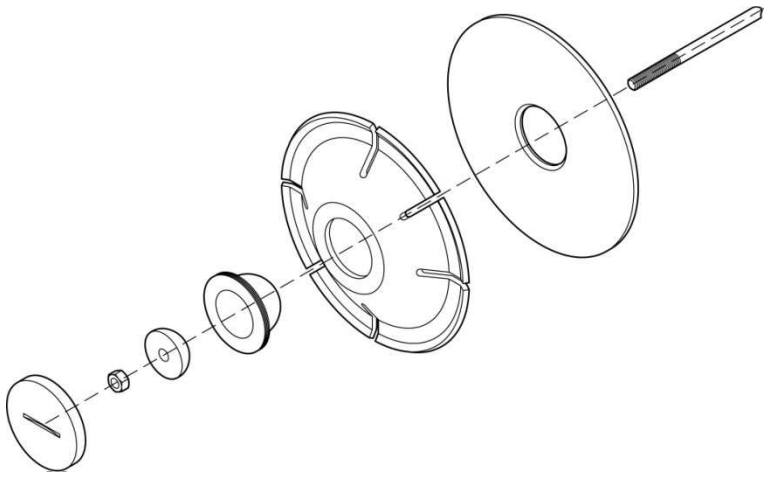

Figure 3 Exploded view of the studied ductile anchor plate connection (Drawing from STAP company)

3 MOTIVATIONS

The latest earthquakes show once again how important connections are between structural elements regarding seismic vulnerability.

Horizontal structural members affect the overall deformability of the structure and the distribution of seismic actions among (according to their in-plane stiffness) and across (according to the boundary conditions) the vertical structural elements. Absence of efficient connections between these structural elements is one of the main reasons for high vulnerability of historical masonry buildings regarding seismic actions.

This deficiency leads to out of plane deformation and then collapse of perimeter walls which is a principal cause of failure in most traditional forms of masonry construction and constitutes the most serious life-safety hazard for this category of building [5].

A schematic representation of the load path in Figure 4 shows that seismic response of structural elements and consequently global behaviour is highly influenced by the energy path which can be disrupted because of deficient connections.

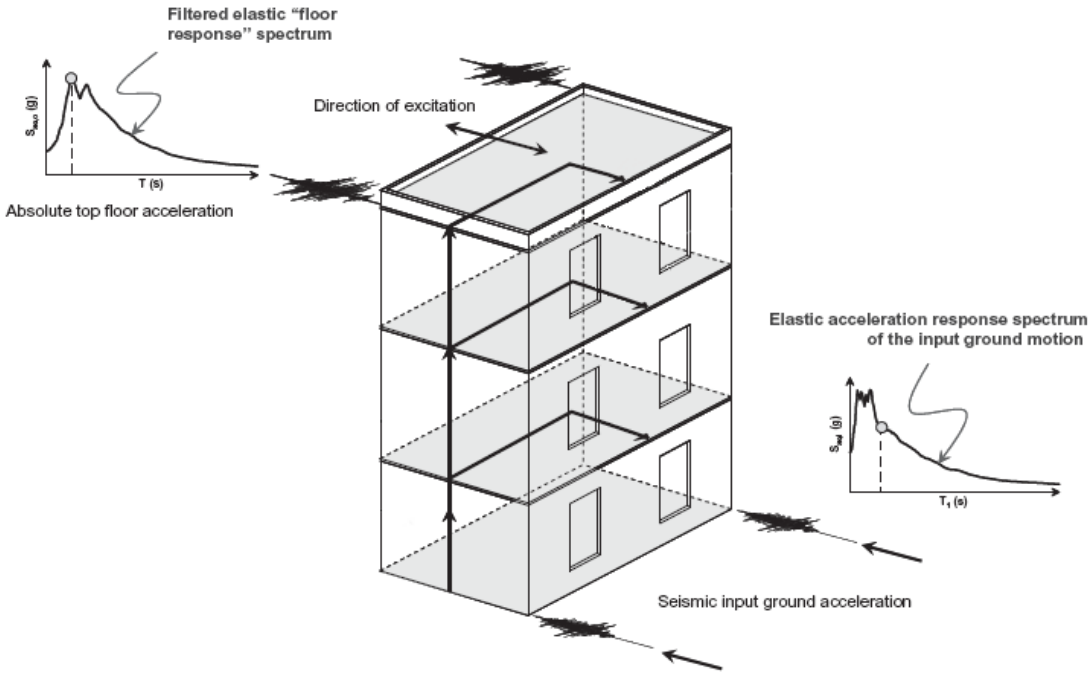

Figure 4 Simplified representation of the energy path and of the filtering effect of masonry buildings on the ground acceleration to walls responding out-of-plane [5]

Despite this important issue regarding seismic performance of masonry buildings, this field has been poorly investigated and more research needs to be done.

4 AIMS

The first objectives of the present study are to understand the seismic response of this structural connection and to demonstrate its contribution and efficiency in comparison with a classical tie rod connection.

If the results show that it really works as an efficient dissipative device, the intended goal is to characterize quantitatively the ductile connection by mean of a stiffness value that could be implemented in a global numerical model of a building.

Such a characterisation of the connection should give more accurate results regarding seismic vulnerability assessment of historical constructions and help engineers and architects to design the appropriate retrofitting method. As it has been said previously, it is highly important to understand both local and global behaviour of a construction in a life-safety hazard analysis.

Finally, a secondary objective is to think about possible improvements that could be made to the anchor plate so this method would become more competitive against other retrofitting techniques.

5 ORGANIZATION OF THE DOCUMENT

The present dissertation is structured in height chapters.

Chapter 1 recalls some background theory about seismic vulnerability in order to point out the global field of the present study and to show the importance of numerical models in nowadays seismic vulnerability assessment. As an introductive chapter, it also describes the topic and defines the objectives and motivations of it.

Chapter 2 presents a state of the art concerning the out of plane failure mechanism in historical buildings subjected to earthquakes and both traditional and innovative seismic retrofitting techniques which can be used to tackle this problem, focusing on the passive protection devices. The literature of non linear numerical analysis applied to FEM is also reviewed.

Chapter 3 introduces the plate by describing the prototype in a qualitative and quantitative way and defines the main expectations of this innovative connection.

Chapter 4 focuses on the main work of the present study which was the numerical analysis of the ductile plate. The preliminary model is fully described and the analysis results are discussed in order to provide a bench mark for the experimental part.

Chapter 5 describes the experimental campaign carried out. The elaboration of the test set-up and the development of the procedure done without any standards are explained and all the experimental results are analysed and discussed by paying attention to the seismic response of the plate.

Chapter 6 explains the calibration process leading to a better matching of the numerical and experimental results. After this comparison and the model update, the final results of the plate are analysed in depth and discussed.

Chapter 7 Analyses the global seismic response of the plate regarding to its connected elements and concludes on how the plate could be improved.

Chapter 8 presents the conclusions and recommendations for further work on this type of ductile connection. An improvement of the plate regarding its seismic response is also proposed.

CHAPTER 2: SEISMIC RETROFITTING OF HISTORICAL CONSTRUCTION

1 INTRODUCTION

1.1 Out of plane behaviour of masonry walls

The out of plane behaviour of masonry walls has been pointed out in several papers as very likely to occur during an earthquake excitation.

Ramos and Lourenço assessed through finite element analyses that the most observed failure mechanisms of ancient masonry buildings due to seismic actions appeared to be the overturning of the perimeter walls [6]. They made the conclusions that in cases where safety against seismic actions was clearly insufficient, owners and regulators must address the issue of retrofitting these structures. They also advised to tie the buildings with steel rods or to strengthen the timber floors, especially taking into account the connections with masonry walls.

Valluzi and Modena confirmed this issue through post-earthquake damage assessment [7]. Their literature review showed that the previous seismic events in Italy, particularly the one in Umbria in 1997 presenting a moderate magnitude (5.6 Richter magnitude scale), led on a large scale to brittle out-of-plane mechanisms of collapses (partial or global overturning of facades or corners) in buildings (Figure 5).

Figure 5 Out-of-plane mechanism observed in unretrofitted buildings [7]

1.2 Important concepts in seismic retrofitting strategies

Seismic retrofitting could be defined as the modification of structures to make them more resistant to earthquake hazard. Seismic retrofit can be achieved by means of appropriate strengthening but alternative strategies can also improve the seismic behaviour of a structure.

1.2.1 Energy dissipation

During a seismic event, part of the kinetic energy provided to the structural system by the earthquake is dissipated by means of frictional forces or structural yielding such as hysteresis which is a form of energy dissipation related to the inelastic deformation of the structure [8].

When a structure is undergoing a seismic excitation, it will amplify the base ground motion according to its ability to dissipate the energy of the earthquake ground-shaking. Regarding masonry buildings, the energy is normally dissipated thanks to friction at the mortar joint interfaces or mortar beddings cracking. This physical notion is very important in seismic retrofitting and it is often that engineers and architects do not pay sufficient attention to it.

1.2.2 Ductility

[2] defines this notion in the context of seismic design as the ability to dissipate energy by developing an inelastic response under high-amplitude cyclic deformations without experiencing a significant loss in load carrying capacity. This important concept does not characterize unreinforced masonry because of the poor bonding strength at the unit-mortar interface. As a brittle material under tension, its lateral resisting capacity is highly affected after the initial damage.

1.2.3 Structural stiffening

Some structures present a weak seismic behaviour because structural elements do not have appropriate ductility or toughness to resist the large lateral deformations induced by the earthquake. Stiffening the structure aims at increasing the seismic performance by reducing lateral deformation. [9] presents different measures to effectively add stiffness to an existing structure such as the construction of new braced frames or shear walls.

1.2.4 Structural strengthening

Structural strengthening is needed is structures presenting an inadequate strength to resist lateral forces explained physically by an inelastic behaviour at very low levels of ground shaking. Adding strength to weak lateral-force-resisting system aims to raise the threshold of ground motion at which damages start to occur.

1.3 Connections

1.3.1 Importance of connections in URM buildings

Most of the time researches focus on structural components like masonry walls or floor and roof diaphragms but rarely on connections between them.

Wall-diaphragm connections can significantly influence the seismic behaviour of unreinforced masonry buildings. Failure of the connections could be the cause for a global structural collapse and their ductility could act on the overall structural response [10].

However, wall diaphragm connections for URM buildings haven't been deeply studied leading to a lack of data on inelastic force–displacement behaviour of wall-diaphragm connections. Force-displacement behaviour, in other words the stiffness values of the connection, could be useful information in order to carry out a numerical analysis of an entire building. One of the main conclusions of [11] is that connections in URM structures affect the overall response of the structure. Therefore, models describing the joist bearing connections should be developed and applied to retrofit designs. They also developed a method to implement dynamic friction behaviour in finite-element models. Friction contributes to the energy dissipation during a seismic event and could avoid a global collapse of a structure.

1.3.2 Main connection types

One of the solutions to increase seismic performance of masonry load-bearing systems is to improve the connectivity between the principal structural members (perpendicular walls and floor diaphragms).

However, improving their connectivity does not lead to either a significant alteration or an important increase of the stiffness of the building. Traditional devices such as anchors or ties are used to improve the connectivity which aims to preserve or even increase the ductility of the retrofitted structure thanks to their flexibility.

At a global level, the main improvements of connectivity focus on intersecting wall connections and wall to horizontal diaphragm connections.

Perpendicular walls can present a particularly weak connection due to cracks present on interlocking bricks bounding and improving their connectivity could lead to a seismic behaviour improvement of the whole structure. An example of retrofitted structure by mean of steel ties is presented in Figure 6. Ties can be positioned in channels cut in the masonry and covered by plaster to be protected from corrosion and both ends are usually anchored with steel bearing plates [8].

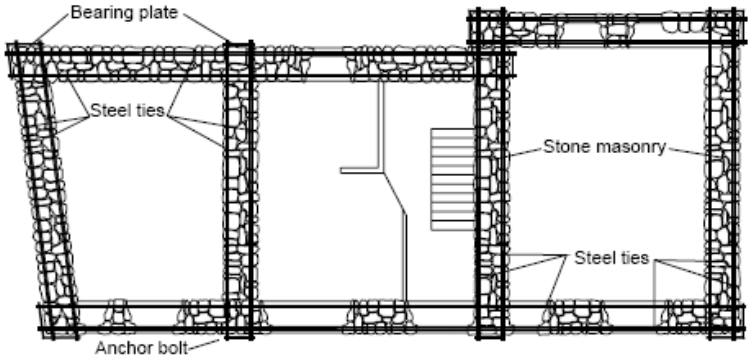

Figure 6 Improvement of perpendicular walls connectivity [12]

Tomazevic et al. (1996) confirmed through an experimental campaign that seismic behaviour of historic masonry houses were depending on the rigidity of floors and connection of walls. They showed that ties prevented out of plane vibration of the wall. They also indicated that lateral load-resistance and deformability, as well as energy dissipation capacity were significantly improved. The comparison of test results pointed out that 2.5-times more input energy was needed to cause the collapse of retrofitted model with steel ties than in the case of the reference model [13].

Another connectivity improvement affecting masonry walls stabilisation and consequently the global seismic behaviour of a structure can be done on walls to floor diaphragms connections. The target is to prevent out-of-plane instability of masonry walls during an earthquake by improving the seismic load distribution through a stiff floor diaphragm. For this purpose, improvement of connectivity may not be sufficient if the floor is not stiff enough. In this case, stiffening of the diaphragm can be carried out by, for example, adding an extra layer of wooden planks on top of the existing floor. Illustrations of alternative solutions for this type of connectivity improvement are given in Figure 7.

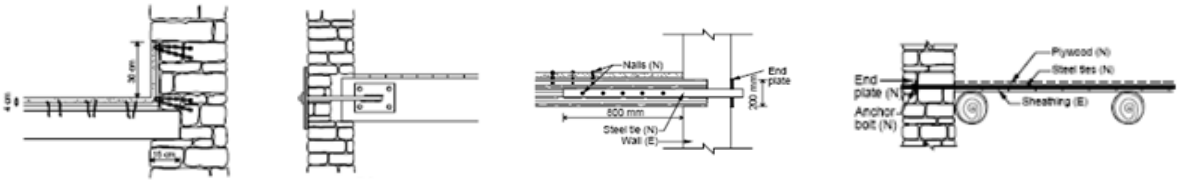

Figure 7 Alternative solutions to connect stiff diagram to masonry walls [8]

1.3.3 Ductile connection design

A state of the art of in connection seismic design is given in [14]. This paper analyses some experimental results concerning rigid or semi-rigid connection in different types of structures mainly steel frames. His first assumption in connection design is that a ductile mechanism in connection or close to it must have a lower resistance than any potential failure mechanism which is brittle or has low ductility in order that the ductile zone will yield before the weak or brittle area. He mentioned another important thing saying that local dissipative devices can provide a stable energy dissipation if their force-displacement relationship is characterized by stable loops.

2 NON LINEAR ANALYSIS OF A STEEL DUCTILE CONNECTION

Design and validation of possible retrofitting techniques can be done through structural modelling by simulating their effect on an accurate numerical model of the structure. Moreover, the analysis of the retrofitted building requires, in particular, the modelling of the retrofitting techniques implemented. Numerical results will then lead to an accurate seismic vulnerability assessment and as a consequence reduce the life-safety hazard.

2.1 Parameters affecting the non-linearity

During a numerical analysis, attention has to be paid to the amount of displacement which occurrs during the loading phase because it will affect the type of analysis. The reason for this is that the stiffness of a structure will be affected by the deformations occurring under a load. If the displacements are small enough which means that the stiffness will not be much affected by the deformation, the analysis can be considered as linear. On the other hand, for higher displacements, several parameters such as shape, material properties or supports can significantly change the stiffness of the structure and, as a consequence, conduct to a nonlinear analysis.

2.1.1 Geometrical non-linearity

Geometrical non linearity refers to the change of stiffness of a structure under a load due to its change of shape. If the deformation is important, the initial configuration might no longer be valid to express equilibrium and compatibility (Figure 8). Moreover, under large deformations, the load direction could change as the structure will deform, depending on the reference coordinate system. Usually, finite element analysis programmes present the choice of following or non-following load.

An accepted rule for the use of a geometrically non liner analysis is given in [15]. It is advised that such an analysis should be used if the ratio of a structure deformation and its largest dimension is greater than 1/20th.

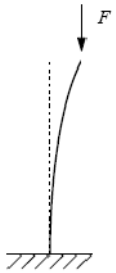

Figure 8 Deformed shape of an element under simple compression [16]

2.1.2 Physical non linearity

Another type of non-linearity analysis is required when the loads are high enough to cause some irreversible deformations to a structure or damage (e.g. cracks). The elastic limit of the material is defined through its constitutive law. Since materials behave in so many different ways, Finite Element

Analysis (FEA) programs have developed specialized techniques and material models to simulate these behaviours. Regarding metals, two material models can be used: Von Mises or Tresca model. The Von Mises model assumes that plastic yielding starts when the elastic energy stored in changes of shape reaches a critical value (Equation 3) whereas the Tresca model is based on the fact that plastic yielding begins when the shear stress on any plane in any direction reaches a critical value (Equation 2) [17]. These two models are shown in Figure 9 in the case of plane stress. The Tresca condition is represented by the six faces of the failure criterion degenerated into lines. The Von Mises condition degenerates into an ellipse passing through the segment intersections which defines the Tresca condition. The intersection of the yield criteria and the axes σ_1 and σ_2 correspond to the uniaxial tensile and compression resistances [16]. According to [18] the Von Mises elasto-plasticity is by far the most widely used plasticity model.

$$\tau_{\max}(\boldsymbol{\sigma}) - \tau_0 = 0$$

Equation 2 Mathematical formulation of Tresca model

$$\sqrt{J_2(\boldsymbol{\sigma})} - \tau_0 = 0$$

Equation 3 Mathematical formulation of Von Mises model

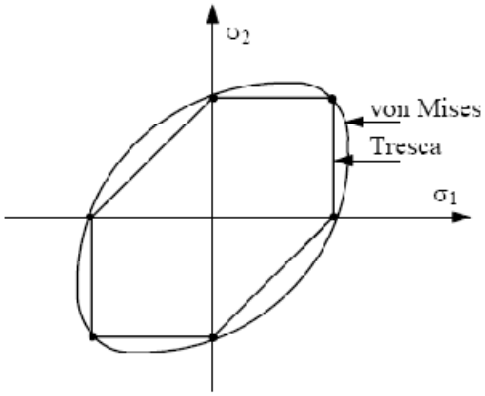

Figure 9 Representation of both yield conditions in the principal stress plane

2.1.3 Contact non-linearity

Changing of the contact or support condition can also modify the stiffness of a structure. This can be easily understood with the practical example shown in Figure 10 where the stiffness is highly affected by the drop of the beam effective length. High attention should be paid to these contact areas. Modelling them should be done by means of contact or interface elements instead of normal supports so that the interacting surfaces can change during the deformation of the structure. These elements are often used and recommended in order to model areas such as bolt and washer or hole for example [19].

Figure 10 Change of effective length of a beam under deformation [15]

The effectiveness of contact elements was demonstrated in [20]; in which different FEM analysis were carried out as well as an analytical analysis and an experimental campaign concerning innovative dissipative connections (INERD). One of their observations on the graph representing numerical results versus experimental ones is that contact element analysis describes in a better way the connection response than the gap element analysis.

2.2 Numerical non-linear solution procedures

The non linear solution procedures are very important in the way that they define the solution in terms of accuracy compared to the real solution and also the time consumption of the analysis.

2.2.1 Types of non-linear procedures

A first solution procedure is based on an increment method. This method called Forward Euler uses the stiffness matrix from the previous load increment in order to calculate the new displacement (Figure 11a) which could lead to an important error.

Another solution procedure, the Newton-Raphson method, is based on the same concept but was improved by using an iteration procedure. In this case, for the same increment of load, the displacement is calculated after several iterations modifying the stiffness until the convergence criterion is fulfilled (Figure 11b).

The last method is called the Modified Newton-Raphson method. As its name indicates, it follows on from the Newton-Raphson method but keeps the same stiffness during each load increment instead of modifying it after each iteration (Figure 11c).

According to [17], in terms of accuracy, the Newton-Raphson method usually implies a fast convergence but each iteration is quite time consuming. On the other hand, the Modified Newton-Raphson method leads to a slower convergence but the iterations are faster.

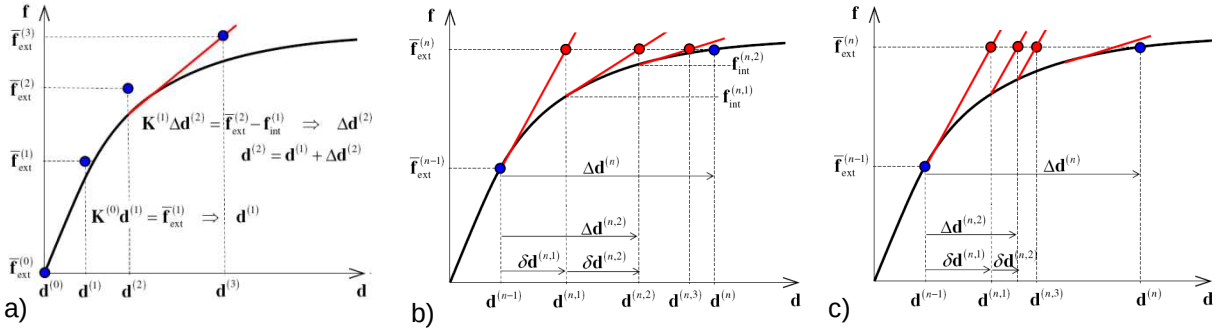

Figure 11 Non linear solution procedures. a)Forward Euler method, b)Newton-Raphson method, c) Modified Newton-Raphson method.

2.2.2 Line search

The iterative procedures aforementioned show a severe limitation by not being globally convergent but converging to a solution from almost any initial solution. To tackle this problem in structural analyses, the line search method is often used to find an estimation of the solution outside of the radius of convergence of the Newton-Raphson method [16].

2.2.3 Convergence criteria

The convergence of the solution method implies the definition of one or several convergence criteria which allow to obtain the wanted solution with the precision wished. The convergence criteria are based on different Euclidian rules and can be divided into three categories depending if the criterion is defined by mean of displacements, forces or energy. The criterion corresponds to the maximum tolerance or error that could be admitted during the calculation to accept the solution [16].

3 PASSIVE SEISMIC PROTECTION DEVICES

3.1 Base isolation devices

The concept of the base isolation aims at disconnecting a building from the horizontal components of the ground motion by mean of a device with a low horizontal stiffness inserted between the structure and its foundations. The horizontal displacements will then be increased but located at the base isolation level (Figure 12). Furthermore, the building will be subjected to a lower acceleration and will hardly undergo deformation behaving as a rigid body.

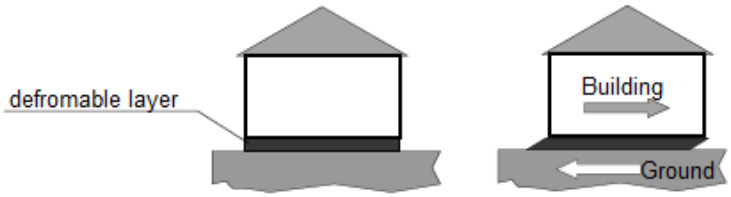

Figure 12 Deformed shape of an isolated building [21]

As a direct consequence the natural frequency range of the building will be reduced. Moreover, isolated structures will also have frequencies lower than the frequencies with the highest energy content of the seismic actions (Figure 13). To be efficient the base isolation device needs to have a good support capacity, a low horizontal stiffness, and both appropriate capacities of energy dissipation and initial position restitution [21].

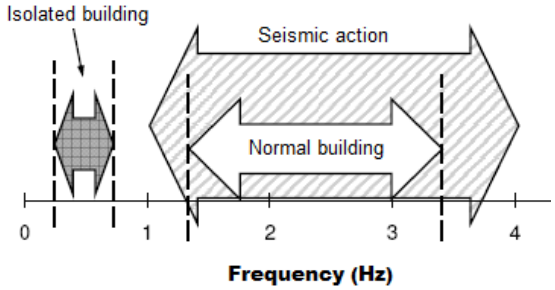

Figure 13 Frequency range of both normal and isolated structures compared to the seismic action [21]

3.2 Energy dissipation devices

Another seismic protection technique is energy dissipation, by means of devices helping the structure in dissipating the earthquake energy. These energy dissipaters are implemented in specific places of the building subjected to relative displacements in order to avoid the structure to dissipate the energy in an autonomous way. Several types of devices exist, the most common being the hysteretic dissipaters and the viscous dissipaters. These two systems have an easy implementation into the structural system and a versatility that favours their use.

3.2.1 Viscous dissipaters

This type of dissipaters works as a piston in which the fluid laminates from one chamber to the other and at the same time dissipates energy. The force-velocity relation will essentially depend on the characteristics of the fluid as shown in the generalized expression (4) taken from [21]

$$F = C|v|^{\alpha} \sin v \tag{4}$$

Where C and α are fluid constants and v corresponds to the velocity.

3.2.2 Hysteretic dissipaters

In the case of hysteretic dissipaters, the energy dissipation happens through the plasticization of the metallic element which is usually steel or through friction of its components. The force will depend on the deformation imposed and the device will be defined by an initial stiffness K_1, a post-yield stiffness K_2 and a yield strength F_T presented in Figure 14. The dissipated energy can be found by calculating the internal area on the graph relating the force and the deformation of the device for each cycle.

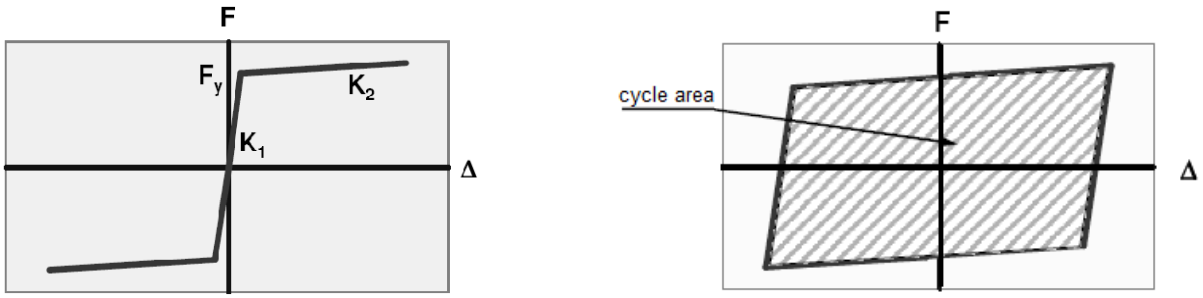

Figure 14 Behaviour of a hysteretic dissipater with its cycle area representing the dissipated energy.

Research has been done in the field of innovative hysteretic dissipaters especially in moment frame connections like the new jointed timber structural system for post-tensioned timber buildings presented in [22]. Newcombe carried out an experimental campaign on jointed ductile connections and concluded by giving guidelines that enable a complete design of post-tensioned timber frame systems. The concept of post-tensionned connection he studied was elaborated in 2004 at the University of Canterbury, New Zealand [23] but the idea of the hybrid connection was conceived based on the existing precast concrete techniques developed at the University of San Diego [24] [25] [26]. This ductile connection shown in Figure 15a was designed so that under a seismic excitation post-tensioned tendons allow a self-centering capacity while remaining elastic and mild steel reinforcements deform inelastically and thus dissipate energy. These two features of the connection lead to a flag shape hysteresis behaviour shown in Figure 15b.

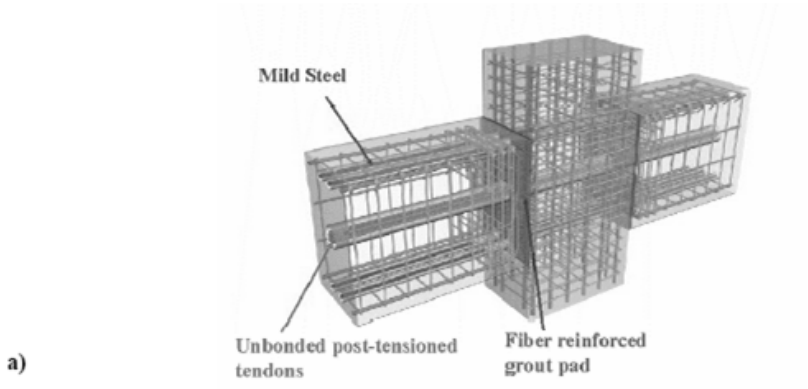

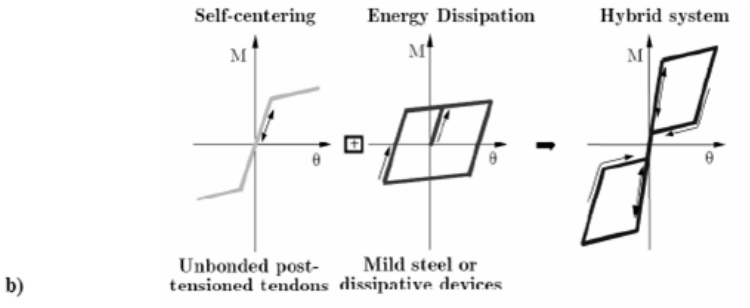

Figure 15 Dissipative connection a) Precast concrete hybrid connection, b) Decomposition of the flag shape hysteresis [22]

3.3 Shape memory alloys

Shape memory alloy devices (SMA) are usually made of an alloy of Nikel and Titanium which are known for their super-elasticity. The dissipation concept is based on the peculiar properties of their material. SMA can undergo important deformation cycles through which they will dissipate energy without plastification of the material nor significant degradation. Furthermore, their great elasticity allows an ecellent recentring of the strenghtenned structures.

As an example, this technique was applied to the bell tower of San Giorgio in Trignano after it had been seriously damaged during the 1996 Modena and Reggio Emilia earthquake. We can see on Figure 16 that four SMA anchoring ties were applied to the structure, increasing its flexural strength [27].

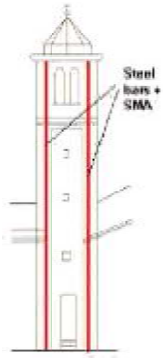

Figure 16 Strengthening of Chiesa of San Giorgio in Trignano

CHAPTER 3: THE DUCTILE PLATE CONNECTION

1 PRESENTATION OF THE PLATE

1.1 Generalities

The innovative connection (Figure 17) analysed in this thesis is based on the traditional anchor plates for tie rods used world widely in most historical buildings with the difference that this ductile plate is designed not only to transfer loads but also to dissipate energy. This concept was brought to light in the NIKER project.

Figure 17 General view of the ductile anchor plate

1.2 NIKER project

The NIKER project is a European project involving both universities and companies dealing with the issue of damages on cultural heritage caused by earthquakes. It aims at complementing and enhancing traditional materials with innovative processes and developing new pioneering technologies. The main idea is that efficient protection of historical heritage should be achieved on the basis of the ‘minimum intervention’ approach.

The project is divided in 10 interactive work packages (WP) going from ‘project management (WP01) to ‘guidelines for end-users (WP10). The present study was introduced in WP06 named ‘connections and dissipative systems with early warning’ in which one of the objectives is to develop a hysteretic dissipation prototype [28]. A first prototype was made by the Portuguese company STAP and this dissertation aims at proving its efficiency and putting in place possible improvements.

2 DESCRIPTION OF THE PLATE

2.1 General description

Instead of being a simple flat plate or even a single bar as in traditional connection, the ductile plate is circular and has a double curved shape with a uniform thickness of 6 mm as shown in Figure 18. It has an external diameter or 250 mm and an internal one of 65 mm. Moreover, six notches of 8 mm wide and 50 mm long are symmetrically disposed every 60° in order to allow the plate to deform and, as a consequence, dissipate energy. We also observe that the external outline is slightly curved toward the top so that the anchor doesn't penetrate the support and keeps sliding and deforming during the cycles of the earthquake excitation. The dimensions are summarized in Figure 18 and they were confirmed during the experimental campaign.

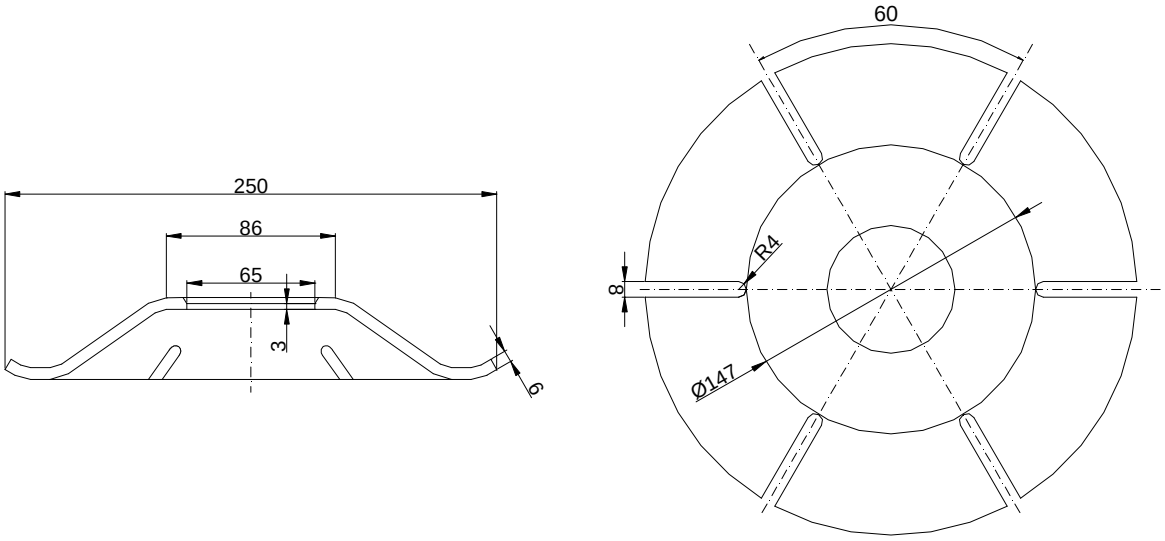

Figure 18 Dimensions of the ductile anchor plate

2.2 Connection system

The exploded view in Figure 19 shows how the connection will be implemented during the seismic retrofitting of the building. The first flat plate (2) aims at supporting the ductile plate (3) with a smooth and strong surface in order to avoid crushing of the masonry before deformation of the connection. Then a system of full and hollow half-sphere (4) transfers forces from the tie rod (1) to the top of the ductile plate which allows the tie rod (1) to have a small rotation and helps the anchor plate (3) to be centre. Finally the tie rod (1) is screwed to a nut (5) and a cup (6) covers the fixation system to protect it and to give an attractive appearance to the whole connection knowing that aesthetic value has also to be preserved in the scope of the conservation of cultural heritage. Once installed, the tie rod can be anchored and pre-stressed in order to confine the structural elements connected (Figure 20)

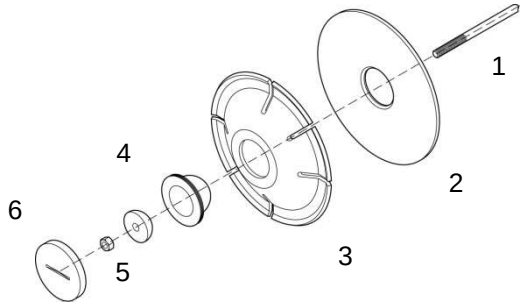

Figure 19 Exploded view of the ductile anchor connection

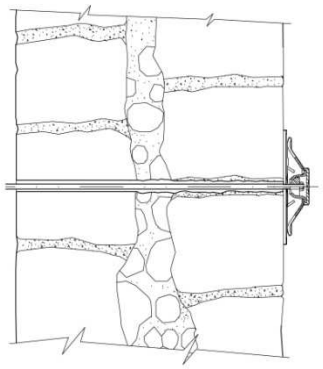

Figure 20 Cross section of a retrofitted masonry wall with a ductile anchor plate

2.3 Expectations

The aim of this innovative connection is to dissipate the earthquake energy at the same time as transferring forces from one structural element to another and as a consequence preserving cultural heritage assets by avoiding or reducing damages to historical constructions that have been retrofitted with this connection.

It is expected that during an earthquake excitation the anchor plate will deform under the cyclic lateral loads and this way will dissipate energy as a spring would do. At the same time, the plate assures a good connection between structural elements like perpendicular walls or walls and floor diaphragms spreading loads and avoiding out of plane deformation of the masonry.

The energy should then be dissipated through hysteretic cycles during the seismic excitation due to plasticity of the material and possibly friction with the supporting plate. This energy dissipation will be represented by the area of the hysteretic loops induced by a cyclic loading on the stress-strain curve.

The other expectation is that even if the latter is confirmed the stiffness of the anchor plate has to be lower than the stiffness of the wall so that the structure is not damaged until the plate is totally squeezed. If this concept is not confirmed, the anchor stiffness has to be decreased or the whole retrofitting technique will act as a traditional anchor plate.

These expectations will be evaluated during the experimental and numerical campaign in chapter 5 and chapter 6.

3 CONCLUSION

Even if traditional anchor plates have proven their efficiency through centuries and earthquakes disasters, this ductile plate could go a step further by adding ductility to the structure with a very similar technique. From the geometry described previously it is easy to understand that the shape of the

anchor was designed to deform and dissipate energy through the plasticity of the plate. This expectation is to be confirmed with the calibrated numerical model in chapter 6.

CHAPTER 4: PRELIMINARY NUMERICAL ANALYSIS

A preliminary numerical model of the anchor plate based on the finite element method has been developed using the software Diana 9.4. A first run of static non-linear analysis was conducted giving a first idea of the ultimate load capacity as a benchmark for the experimental campaign. This chapter describes the modelling procedure carried out before the experimental campaign. The calibration of this model will take place in chapter 6.

1 DESCRIPTION OF THE MODEL

1.1 Model geometry

The geometry was first imported from an AutoCAD drawing given by the company STAP that designed and manufactured the prototype. All the dimensions of the drawings detailed in the chapter 3 were controlled according to the real plate using a calliper rule. For each dimension three measures were taken in order to obtain a consistent average. The error observed for each averaged dimension was less than 2% which confirmed that the drawings were in accordance with the real plate. The summary of these measures can be found in annex 1.

Only a sixth of the full plate was modelled to begin with because of its shape complexity and its axi-symmetry. It was then copied six times rotating around the axis of symmetry but only once the geometry and the mesh were finished in order to avoid repetitive work and to save time.

Surfaces and body were created from the points and lines imported from the AutoCAD drawing in order to be able to mesh the plate in the next step of the modelling phase.

In addition to the plate, a ring through which the load will be applied was also modelled by means of a cylinder with a thickness and a diameter able to reproduce the contact area of the plate and the fixation system. This ring can be seen in Figure 21Figure 29.

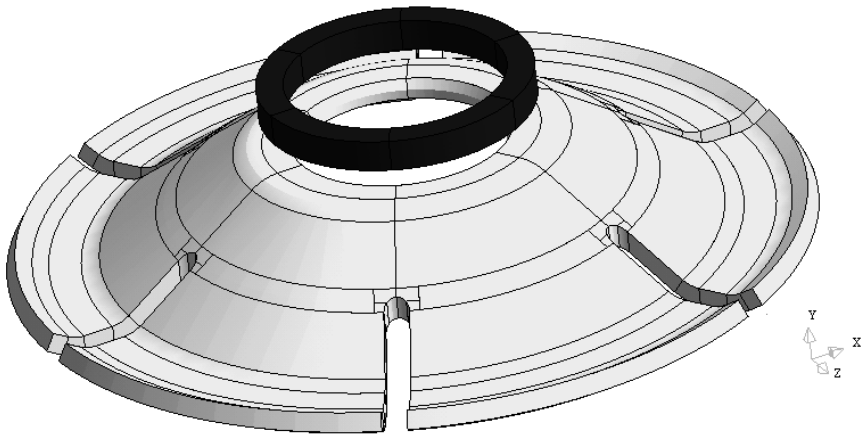

Figure 21 Final geometry

Special attention has to be paid during this first task in order to avoid large changes once the model is almost finished. The user has to think of all the next steps and see how he will mesh the plate or apply the load because, for example, it might need extra bodies or surfaces for this purpose. This will be detailed in the following sections dealing with openings and interfaces.

1.2 Model mesh

1.2.1 Mesh elements

1.2.1.1 General mesh elements

The whole plate was meshed with CHX60 elements presented in Figure 22a. This element is a 20-nodes isoparametric solid brick element and has for basic variables the translations u_x u_y and u_z in the local element directions (Figure 22b). Then, the derived variables are the Green-Lagrange strains and the Cauchy stresses [29].

Figure 22 CHX60 element a) Overview of the element b) Basic variables

1.2.1.2 Contact/interface elements

Contact and interface elements allow two different bodies not connected to interact and describe the interface behaviour in terms of a relation between the normal and shear tractions and the normal and shear relative displacements across the interface [29].

For this preliminary model, only the contact between the anchor plate and the ring applying the load have been created by means of these elements. More precisely, interface elements called CQ48I were used to create an interface between the two surfaces. This element is a plane quadrilateral with 8+8 nodes and is designed for 3D problems (Figure 23).

Figure 23 CQ48I element a) Overview of the element b) Basic variables

The easiest way to model them was to create a body between two surfaces that would interact, attach the wanted properties and then move both surfaces on top of each other before meshing the whole model.

1.2.2 Mesh algorithm

Since the plate has a double curved shape the only meshing algorithm available was a mapped algorithm based on the body edges division. This algorithm produces a conventional mapped mesh for three- and four-sided surfaces [29]. As a consequence, opposite surfaces needed to have the same number of divisions which made the mesh harder to control and refine.

1.2.3 Mesh size

To get more accurate results, the choice of two layers in the thickness has been done as shown in Figure 24. For example, if the top layer is in compression during the loading phase, the bottom layer will be more likely to be in tension and this way the model will give more accurate results. For this purpose, the body edges corresponding to the thickness of the plate were divided in 4 because each brick edge needs 2 divisions to be meshed (Figure 22).

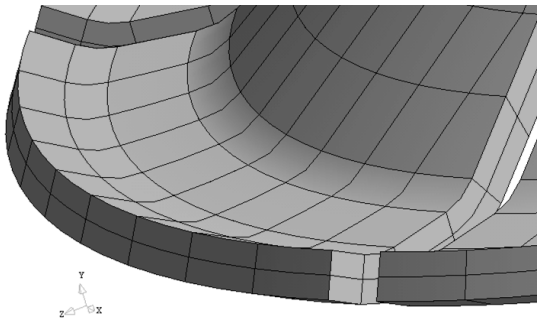

Figure 24 Detail on the two layers of elements in the thickness of the plate

In terms of size, the solid brick element dimensions in the three axial directions X, Y and Z needed to be of the same order of magnitude [29] and if this characteristic wasn't fulfilled, the mesh quality test would warn us. In our case, the mean element size is around 6mm x 6mm x 3mm.

1.2.4 Detail of the openings

The notches were very delicate areas to mesh because of their irregular geometry which could lead to a much distorted mesh. Moreover, a high concentration of stresses was expected in these regions so a bad mesh would affect the overall behaviour and the final results. In order to tackle this problem, a quick analysis of two models with different disposition of additional bodies around the openings was carried out and the more realistic one was retained.

1.2.4.1 Model 1 with one quadrilateral-based and two triangular-based bodies

This model was meshed with wedge elements with very sharp angles leading to a high concentration of stresses during the analysis in these elements (Figure 26). Since cracks were more likely to propagate in the centre of the notches rather than on the sides, this model didn't seem very appropriate. These results confirmed the quality test of the mesh performed which mentioned these elements to be badly shaped (Figure 25).

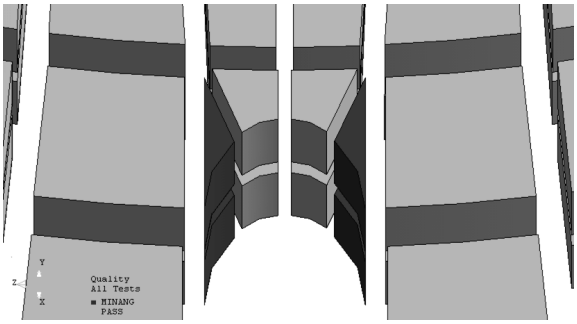

Figure 25 Detail on the mesh quality test

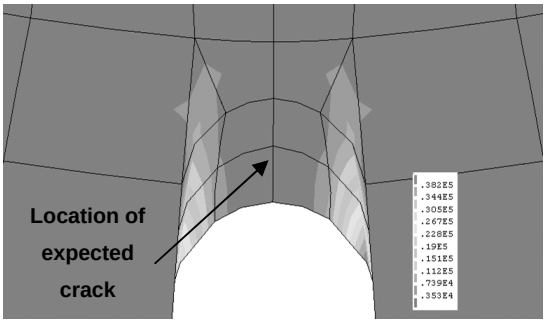

Figure 26 Nodal principal stress P1 for model 1

1.2.4.2 Model 2 with three quadrilateral-based bodies

For this model the three quadrilateral based bodies were meshed with brick elements which all passed the quality test during the meshing phase (Figure 27). Moreover, the results of the short analysis carried out showed a higher concentration of stresses in the centre of the notches (Figure 28) confirming our expectations of crack formation in this area.

Subsequently, the model 2 was then preferred for the rest of the study.

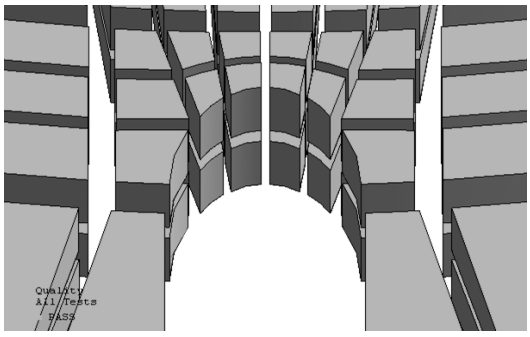

Figure 27 Detail on the mesh quality test

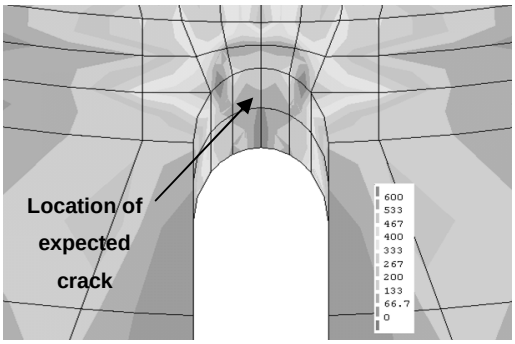

Figure 28 Nodal principal stress P1 for model 2

1.2.5 Final mesh

An overview of the shrunken mesh is presented in Figure 29 to have a general idea of the meshed ductile anchor plate and of the ring applying the load. It can be observed that all the elements passed the mesh quality control.

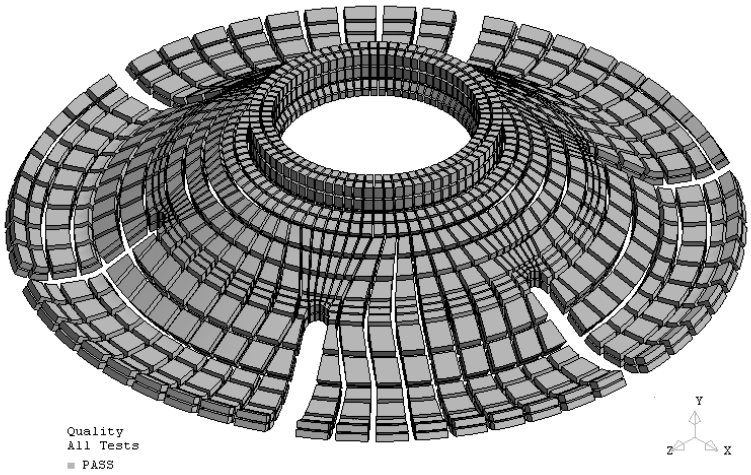

Figure 29 General view of the shrunken mesh of the ductile anchor plate

1.3 Model properties

The next step after meshing the geometry was to attach all the properties to the elements such as material properties, boundary conditions and loading. These parameters will most probably be the ones that will be affected during the calibration of the model in chapter 6.

1.3.1 Material properties

1.3.1.1 Steel property

Together with the boundary conditions, the material definition is an important parameter that can easily influence the results. Since the company STAP was not able to provide us with these characteristics, the best way to define the material constitutive law would have been to perform some tensile tests on standard coupon samples but for a question of time this was not possible.

To determine the steel characteristics for the model, the assumption of stainless steel *aisi 304* has been made. The constitutive law of this material was firstly defined as elastic isotropic with a Young modulus of elasticity of 210GPa and a Poisson ratio of 0.3. Regarding the nonlinearity of the material, the steel was characterized by mean of a Von Mises plasticity with a work hardening diagram shown in Figure 30. This chart was constructed with a yield tensile strength of 210MPa and an ultimate tensile strength of 505MPa.

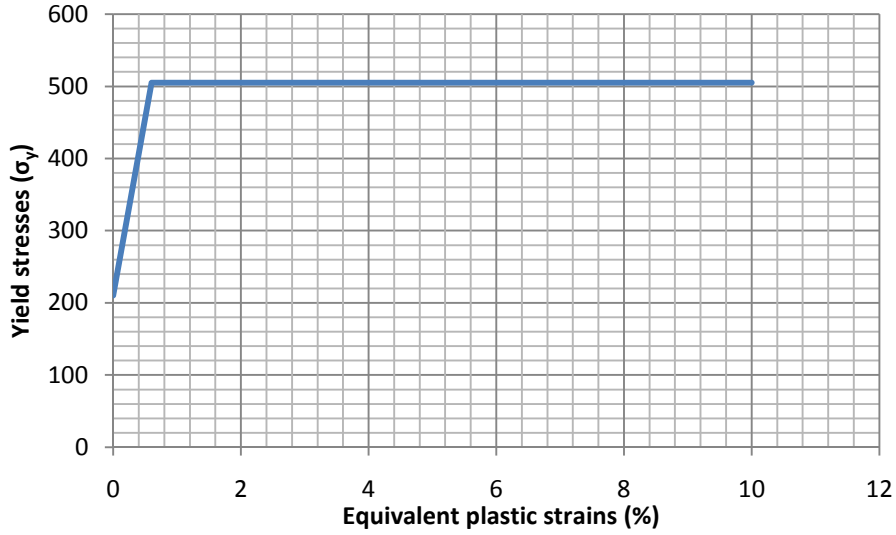

Figure 30 Uniaxial stress strain diagram with work hardening

1.3.1.2 Interface elements material property

Interface elements were modelled between the top of the plate and the ring applying the load. The material property attached to these special elements was first defined with a linear elasticity by means of a linear normal stiffness of 1GPa and a linear tangential stiffness 10^6 times smaller. In addition, a static nonlinearity was added to characterize the nonlinear friction with a cohesion equal to zero and a friction angle of 30°. But during the cyclic analysis, it was observed from the resultant forces of the supports being negative that the ring was pulling the plate up instead of just releasing the load. The reason for this was that the linear stiffness was valid not only for compression but also for tension. As a consequence of this tensile stiffness, the ring was transmitting the negative displacement to the top of the plate.

In order to solve this problem, a non linear stiffness was attached to the interface elements instead of a friction model. This assumption allowed two different behaviours for the normal stresses. The compression was modelled with an infinite stiffness whereas the tensile resistance was expressed with an almost zero value. Moreover, the frictional model was characterized through a symmetrically non linear tangential diagram.

These properties were highly expected to be modified during the calibration depending on the results obtained.

1.3.2 Boundary conditions

In place, this ductile plate will be supported by another flat steel plate which will create a stiff and smooth contact. As a simple assumption, this has been modelled by means of vertical supports (in Y direction) on the contacting line at the bottom of the plate. It is expected that during the calibration of the model this boundary condition might need to be changed for contact or interface elements with

friction behaviour because when the plate starts to be squeezed and to deform, the contact surface changes whereas in this assumption it always stays the same. The experiments will give more information about this.

Moreover, to get a stable model during the analyses, one node on top of the plate has been fixed in horizontal directions (X and Z) so that the plate doesn't move away from its initial position.

1.3.3 Loading

As explained in chapter 3, the load will be applied by this full hollow half-sphere system so a similar ring has been modelled to apply the load, connected with interface element to the ductile plate. For analysis purposes, the load is implemented on this ring by means of negative displacements in Y direction.

The type (monotonic or cyclic) and the speed of the load are defined during the analysis phase through the load step increment. This will be discussed in the following section.

2 ANALYSIS

2.1 Type of analysis

The analyses were carried out as physically non linear analysis in order to take into account the nonlinear behaviour of the materials and also because interface elements impose this kind of analysis. Regarding the non linear solution procedures, regular Newton method with line search was used in order to have accurate results and to improve the convergence of the steps.

The output files were resized by asking to calculate only nodal displacements (global translations), nodal reaction forces, green strains, averaged Cauchy stresses and averaged Von Mises stresses.

By only changing the procedures corresponding to a monotonic or a cyclic loading, two analyses were run under displacement control.

2.2 Procedures

2.2.1 Monotonic loading

The monotonic loading was implemented through linear procedures going from 0 to 20mm increasing 1mm per step with finer steps of 0.5mm during the elastic phase. The regular Newton method with a maximum of 100 iterations was used for each load steps. This method gives a fast convergence of the solution but each iteration is quite expensive. Moreover, only the energy parameter with a convergence tolerance of 0.001 was used as a convergence norm.

2.2.2 Cyclic loading

The cyclic loading procedure was more delicate because of convergence problems, especially during the short moment in between the loading and unloading phase creating peaks on the force displacement diagram. For these load steps, the non linear solution procedure was changed to the linear method so the solution would not diverge.

In terms of load steps, the displacement applied was also in the range of the millimetre, and sometimes smaller in order to improve the problem of convergence of the solution.

2.3 Plotting the results

Two of the main interesting parameters in the discussion of the results were the maximum displacement of the structure and the force applied to get this displacement. Moreover, the FEA software Diana extracts the results in tables giving the asked data for each step. The first problem to get these data was that the loading was based on an imposed displacement procedure so the force was unknown. In order to get the equivalent external force corresponding to each displacement, it needed to summarize all the support reaction for each step. The second problem was that all the data collected from the FEA software Diana were ordered in terms of steps and not in terms of node so to plot a graph corresponding to a nodal displacement in a 500 steps analysis for example, it was needed to go through all the steps to get the wanted data. To solve these two problems, two macros have been created in Excel, one extracting the nodal external reactions and summarizing them for each step, and the second to extract the nodal displacement for each step.

3 PRELIMINARY RESULTS

3.1 Ultimate load capacity

This preliminary analysis aimed to have a first approximation of the ultimate load capacity of the plate in order to choose the right testing machine according to its capacity and to do a good calibration of the testing procedure during the experimental campaign. In order to get this information, a graph reproducing the equivalent load applied versus the maximum displacement located on the top of the plate was plotted (Figure 31). The load capacity of the specimen can be determined by observing the shape of the curve. The graph shows a first behaviour up to 2.5mm during which the load and the displacements increase linearly. The second behaviour of the plate corresponds to the plastic phase. For a very small increment of load, the displacements are much more important because the stiffness of the plate has been drastically decreased. The force corresponding to this plateau is the ultimate load of the specimen, which in this case is equal to 130kN. Moreover, a trend line was added to the linear part of the graph in order to determine the initial stiffness of the plate which can be observed around 55kN. The final results will be more deeply analysed in chapter 6 once the model will be calibrated because the results will be much more accurate than the approximated ones in this section.

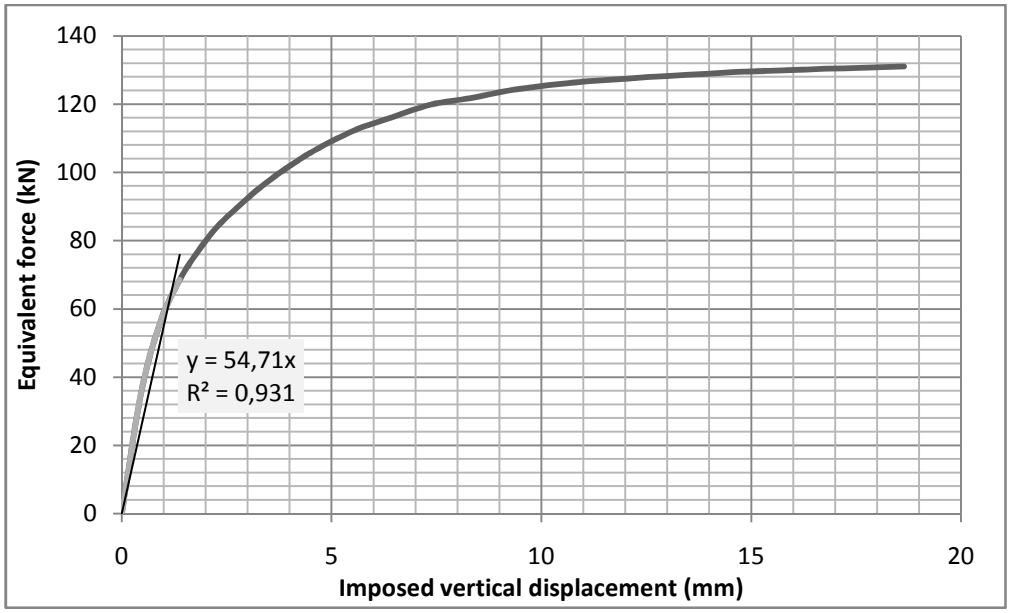

Figure 31 Force versus imposed displacement for the preliminary model

3.2 Expectations during the experimental campaign

3.2.1 Deformed shape

The final deformed shape shown in Figure 32 gives an idea of how the plate will deform during the test. For example, it can be seen that the maximum vertical displacement is equal to 22mm so the LVDTs measuring the vertical deformation during the experiments will have to be chosen in this range in order to get accurate results. The same results were analysed for horizontal displacements.

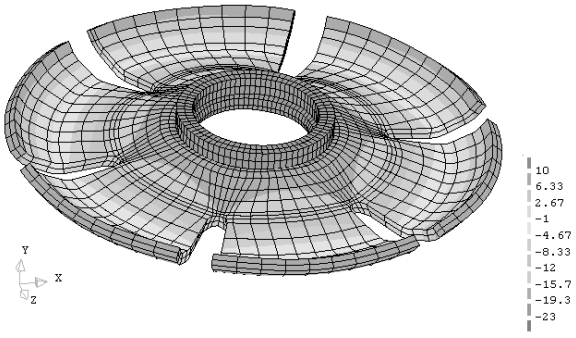

Figure 32 Vertical displacements plotted on the deformed shape

3.2.2 Distribution of stresses

Another preliminary result interesting to analyse in order to predict the experimental campaign was the distribution of the stresses. First of all, the stresses were not equally distributed along the supported line so the boundary conditions had to be carefully analysed during the experiments. Moreover, a high

concentration of stresses was observed in the notches so attention had also to be paid on this area where cracks were possibly going to form.

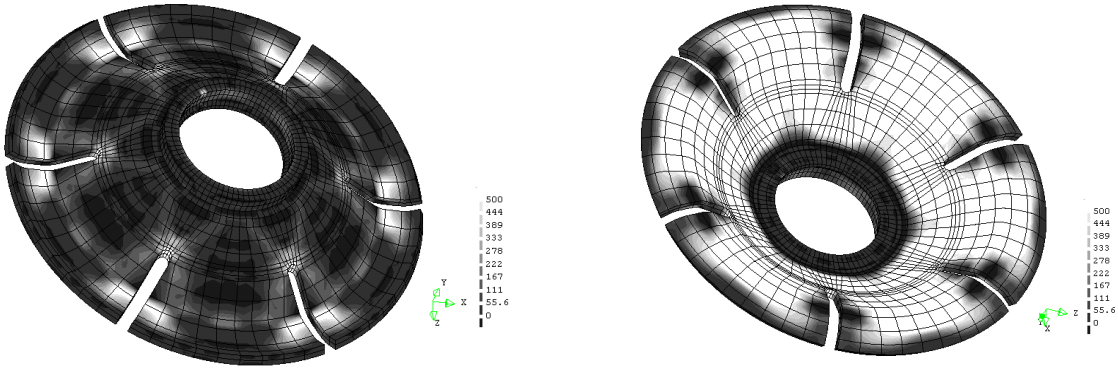

Figure 33 Top and bottom view of deformed plate with principal stress 1 from 0 to 500MPa

4 CONCLUSION

A preliminary model was developed in order to give a bench mark for the experimental campaign and to have a base for the calibration of the model. During the plate modelling, which was one of the main parts of this study, several problems were encountered, the first one being creating an accurate mesh of the singular double curved geometry. Still in the modelling part, the implementation of the properties for the steel material and the interface elements was not easy and thorough researches were needed to understand the right way to recreate reality in the model. The literature review concerning non linear analysis has been of a great help in terms of procedure development with solution procedure methods to determine the analysis type and its parameters.

Regarding the results, the ultimate load found around 130kN was used as a bench mark for the experimental campaign and the response of the plate during the monotonic analysis helped to select LVDTs with an appropriate range. The distribution of stresses was also interesting in the way that it gave hints on the location of sensitive areas to pay attention to.

CHAPTER 5: EXPERIMENTAL CAMPAIGN

1 TEST SET-UP

The experimental campaign carried out was not described in any standards so the test set-up and the procedure were elaborated to match as closely as possible the study of this innovative connection.

1.1 Test overview

Seven compression tests were carried out with the 500kN capacity hydraulic jack of the civil engineering laboratory of the University of Minho. More precisely, one was tested under a monotonic load to obtain the ultimate load of the specimen and then the six others were subjected to a quasi-static cyclic loading in order to study the seismic behaviour of the ductile plates.

The displacement controlled load from the hydraulic jack was transmitted through the real connection system of the anchor detailed previously to the top of the plate by simple contact in between the load cell and the ring. The mean speed of the displacement applied was 50 µm/s.

In order to create test conditions easy to model and close to reality but without affecting the expected results concerning the plate itself, the specimens were compressed on a thick steel plate with a smooth surface. As a consequence, the plates were simply supported in the vertical direction with no horizontal constraints other than friction.

Vertical displacements on top of the plate and horizontal ones on the outline perimeter were measured over three different points for each parameter by means of two home-made systems. Moreover strains on the top and bottom surface of the plate were determined with the use of strain gages. All these can be seen in the following drawings on Figure 34. All instrument readings were recorded using a data acquisition system.

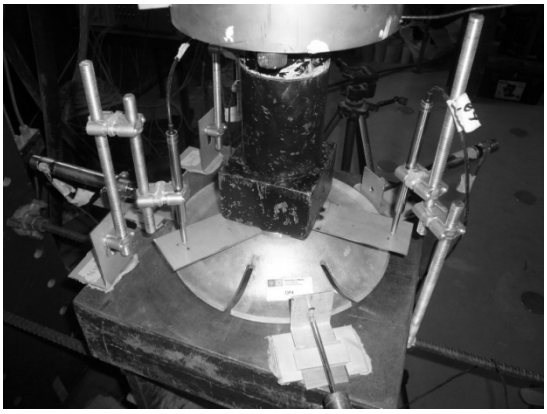

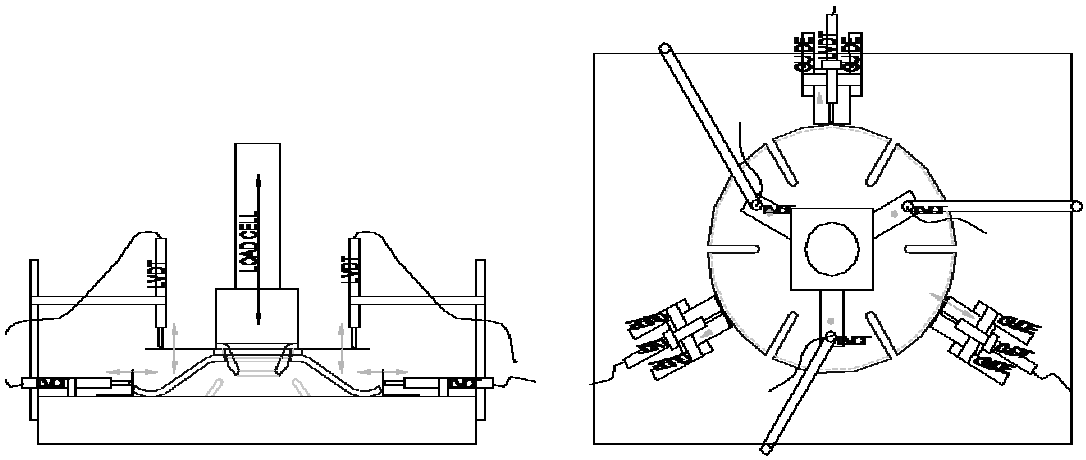

Figure 34 Measurement set-up

1.2 Test instrumentation

In order to make an accurate calibration of the model, it was necessary to record as much data as possible during the test to be compared with the model. After analysing the preliminary numerical results, it was decided to measure vertical and horizontal displacements of the plate outlines by means of LVDTs, and strains in an area where stresses were reasonable to determine with the use of strain gages.

1.2.1 Testing machine

The preliminary results from the numerical model were useful in order to determine the appropriate testing machine comparing its maximum capacity with the plate's ultimate load. Since the latter was found around 130kN with the numerical mode, it was decided to use a hydraulic jack with a maximum capacity of 500kN, with both possibilities of load and displacement control.

Figure 35 General view of the testing machine and zoom on the hydraulic jack.

1.2.2 Strain gages

The strain gages were connected to the measuring device which had to be set depending as to whether it was recording compression or tension strains. Their implementation will be demonstrated in the next part “preparation of the specimens”.

1.2.3 LVDTs

Once again, the numerical model was used to determine the expected displacement in order to choose LVDTs corresponding to the appropriate range of displacements. The maximum value for the horizontal displacement was found at 7mm so ±10mm LVDTs were chosen. Moreover, since the plate is 22mm high, the maximum vertical displacement was not going to reach more than 20mm so the same ±10mm LVDTs were used.

Measuring the horizontal and vertical displacements was delicate because the deformation of the plate induces some rotation so all the translations of the outlines are composed of horizontal and vertical components. Their implementation can be seen Figure 34.

1.3 Preparation of the specimens

1.3.1 Geometry checking

As explained during the geometry modelling phase in the next chapter, the geometry was measured by means of a calliper to confirm the drawings. This task could also be useful if one test appeared to be different from the others, so that the geometry parameter could be excluded from the causes of this difference. The summary of these measures can be found in annex 1.

1.3.2 Preparation of the surfaces

The specimens were fabricated by the company STAP with the use of moulds. For this reason, they had surface imperfections. In order to get a regular surface and to be as close as possible to the model, these irregularities on the supported area, and where the load was applied, were sanded down by mean of a smooth half-round file and cleaned.

Finally, all plates were numbered from DP1 to DP7, with DP as an abbreviation for Ductile Plate.

1.3.3 Positioning of stain gages

It was decided from the numerical model to put the strain gages between two openings, at a distance of 40mm from the top hole of the anchor plate, region where the model was giving reasonable values to be measured.

Once the position was marked, the strain gages were strongly glued on a sandpapered and polished surface after which another layer of resin was applied as a protective layer.

Figure 36 Specimen preparation: a) surface sanding, b) numeration, c) geometry

2 PROCEDURE

Before starting the test, the specimen was first centred with the load cell so that the load was applied symmetrically to the plate. Then the LVDTs were put in their range and the load cell was lowered until it was just touching the top ring of the anchor. After this, the test could start.

The load steps were applied by mean of displacement rated with a speed. Two different procedures were introduced depending on the type of test carried out.

2.1 Monotonic test

The procedure was linear with a speed of 10µm/s and was stopped manually when the hollow half-sphere from the fixation system was about to touch the supporting steel plate.

2.2 Cyclic test

Each cycle was repeated twice with the same speed during the loading and unloading phase except for the last three cycles going up to 12.5mm, 15mm and 20mm which had a loading speed of 50µm/s and an unloading speed of 0.1µm/s. The elastic domain going until 5mm was loaded with a speed of 10µm/s and the plastic domain with a speed of 50µm/s, representing a total of 20 cycles and a duration of 4000s.

The cyclic procedure chart shown in Figure 37 gives a visual overview of the load applied to the specimens. While the plate was behaving elastically, each cycle was going back to 0.5mm but once the anchor was not recovering its initial shape due to plasticity, the minimum displacement value of the cycles was increased so that the plate was not totally unloaded. This procedure was adjusted from the first two cyclic tests carried out.

The whole history of the different cycles is detailed in annex 2 presenting for each step its duration, speed, displacement aimed, and accumulated time.

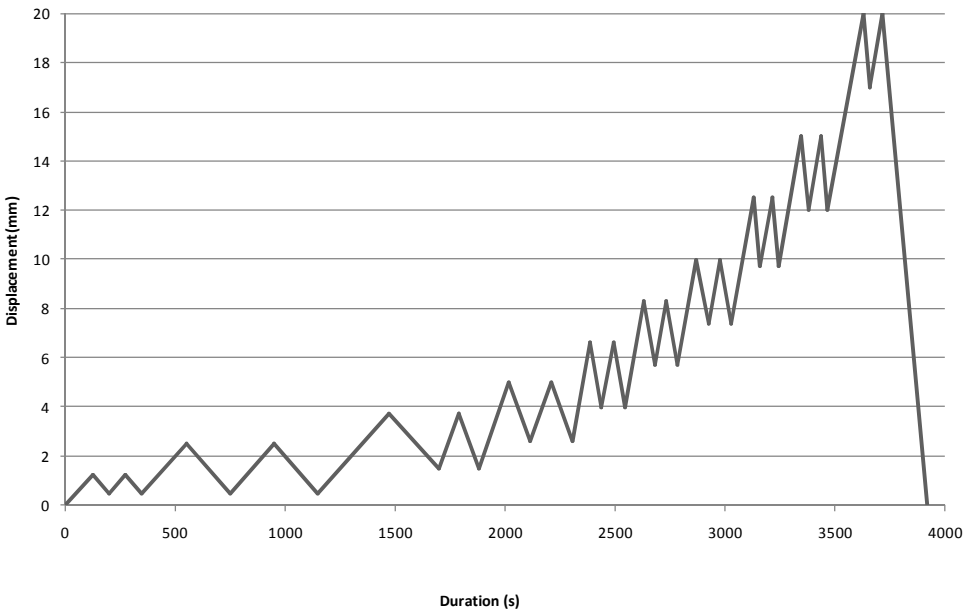

Figure 37 Cyclic procedure represented in terms of displacement and duration.

3 RESULTS

For a better understanding of the results, a qualitative comparison between the initial and the deformed shape of the plate will be discussed before analyzing the data given by the acquisition system.

3.1 Description of the deformed shape

3.1.1 General shape

The compressed plate could be assimilated to a flower fully developed. As expected, the opened notches helped the specimen to be squeezed. As a consequence, the inner part went flat (from 42mm to 22mm) and the outline perimeter increased from 250mm to approximately 265mm (4%). At the same time, the six petals rotated upward bringing the outline from a height of 12mm to 22mm

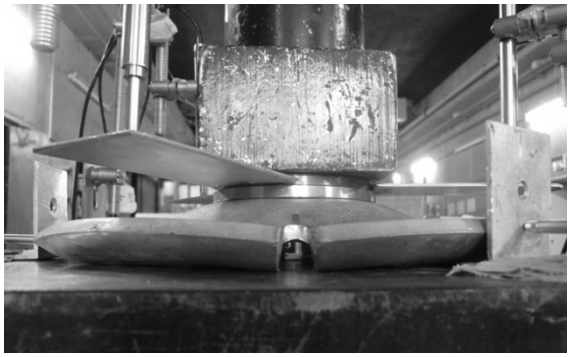

Figure 38 Overview of the deformed shape (left before loading, right after loading)

By looking more precisely at the deformed plate, it seems that the specimen ended up behaving as six petals. The separation of each petal shown in Figure 40c occurred which modified the boundary conditions. At the beginning of the test, the plate was supported along a line but the supports became punctual on the sides of each petal after a few minutes which can be clearly seen on Figure 39b. Figure 39a show the steel located on these corners crushed due to a high concentration of stresses. The top ring where the load was applied also suffered this phenomenon through small “waves” presented in Figure 39c. Each of these waves corresponds exactly to the curved petal.

Attention has to be paid to the support problem during the implementation of this anchor on a building because with a masonry wall the load will be transferred through twelve points instead of a whole line and the masonry will be crushed before the steel. Therefore a second flat steel plate between the ductile plate and the wall is needed.

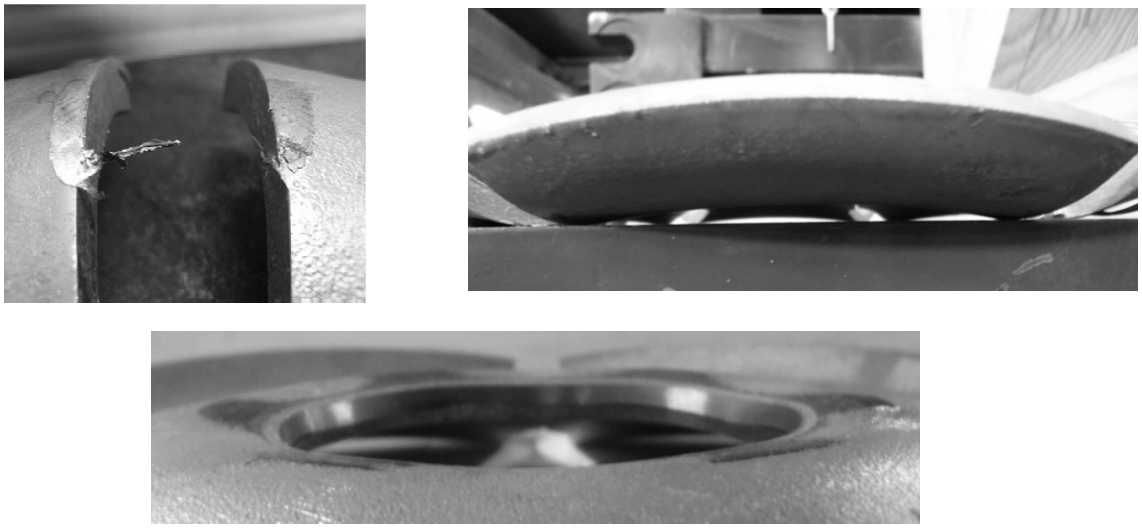

Figure 39 Separation phenomenon a) Crushed corners b) Bottom Curve c) Waves on top ring

3.1.2 Cracks

As expected, a concentration of stresses occurred in the end of the notches leading to cracked material. These geometrical irregularities were made on purpose in order to help the plate to open and then dissipate energy. The first micro cracks appeared around 80kN and were more distinguishable when the imposed displacement reached 12mm. Starting from the bottom of the plate which was in tension as predicted, the cracks propagated in the direction of the top of the specimen, as shown in Figure 40b. By passing the finger across this area, it is easy to feel that the thickness has decreased in this area which means that the steel was yielding and that the crack was likely to continue. The crack propagation directions and the yielding areas seem to confirm that the plate aims to behave as six parts attached together by the top ring and will stop behaving as a whole as soon as the steel starts to yield.

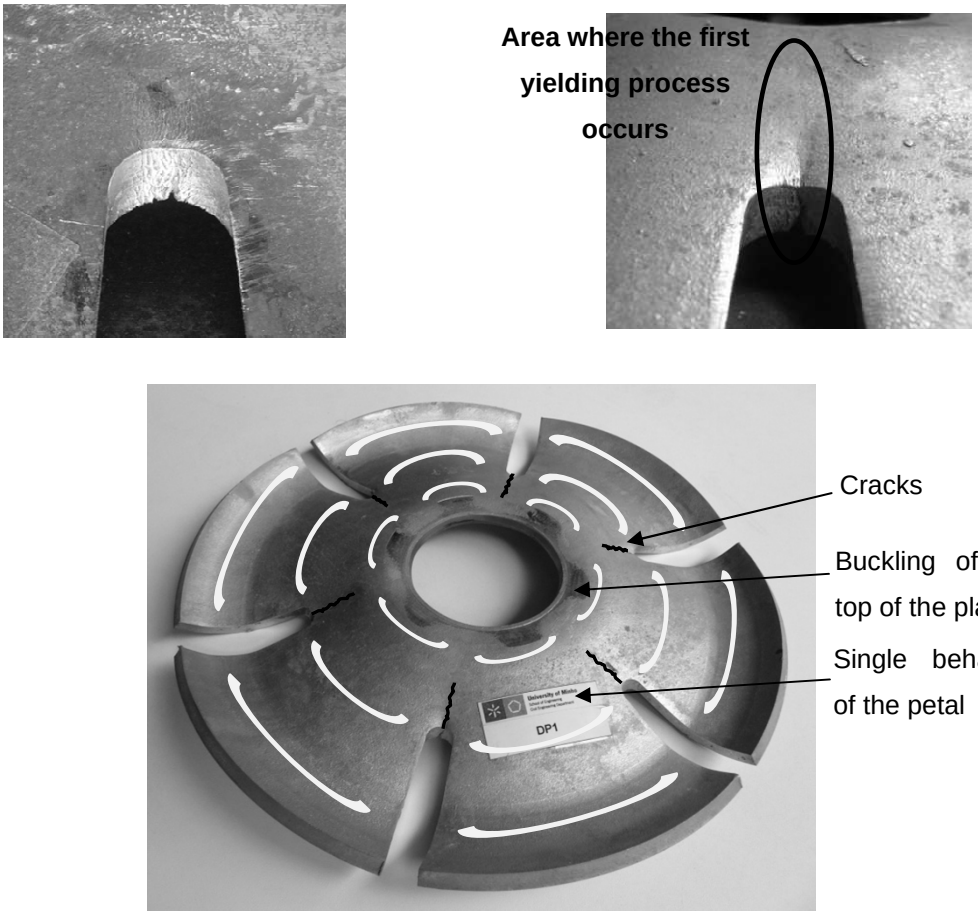

Figure 40 Yielding phenomenon a) Micro cracks b) Propagated crack with yielding area c) Global behaviour

3.2 Ultimate load capacity

The first confirmation of the preliminary numerical calculation of the ultimate load capacity was made through a monotonic test. One plate (DP6) was subjected to a quasi-static monotonic load until the specimen was totally squeezed. Figure 41 shows how the applied force is related with the top vertical displacement of the specimen. We can clearly observe on this graph four different behaviours with transition phases from one to the other.

- Behaviour 1: Corresponds to the elastic range with a high stiffness, during which the specimen could recover its original shape if the cell was unloaded. The stiffness starts to change for a load around 70kN and a displacement around 3mm.
- Behaviour 2: Defines the hardening process of the steel, the stiffness is highly decreased due to the plasticity of the material but the specimen still has a small load bearing capacity. This drop in stiffness could also be explained with the non-linearity of the geometry which is changing during the test. At the end of this phase the plate reaches its ultimate load capacity which is almost 90kN for a displacement of 12mm.
- Behaviour 3: Characterizes the non-linearity during which the specimen no longer has a load bearing capacity. This behaviour took place during the last 10mm of the test.
- Behaviour 4: This peak has nothing to do with the specimen. It corresponds to the moment when the ring applying the load reaches the non deformable base supporting the plate. The test was then stopped.

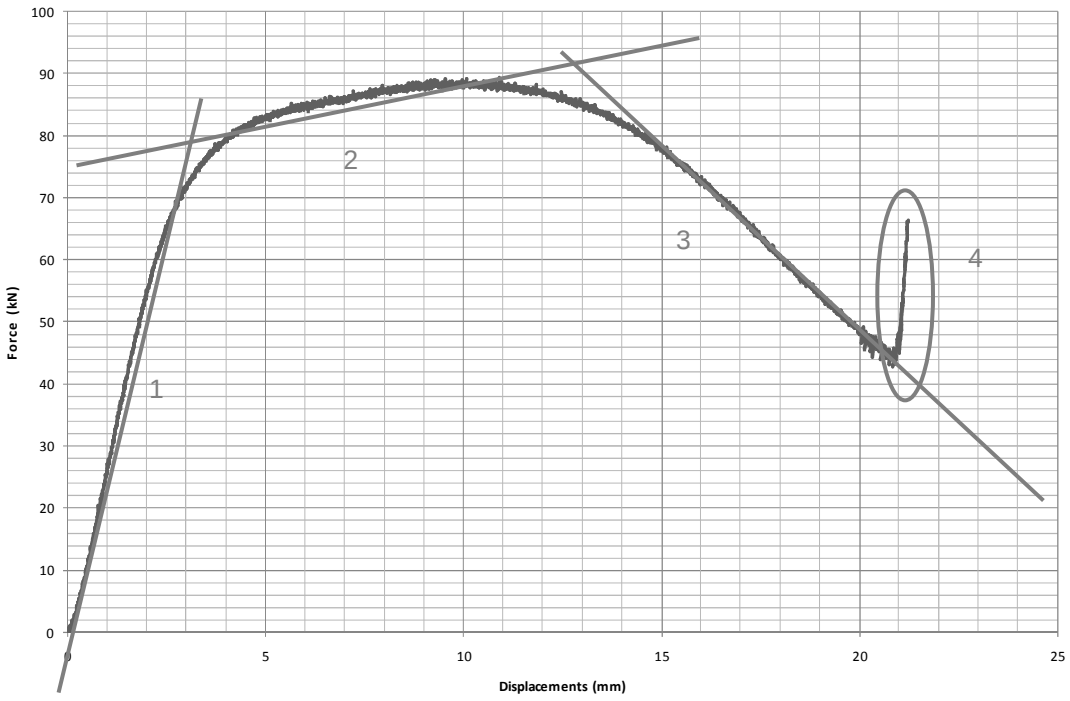

Figure 41 Force-displacement relationship of the specimen DP6 tested under a monotonic load

To summarize, the specimen stayed in the elastic range until it was squeezed to 3mm corresponding to a load capacity of 70kN. Then micro cracks started to appear between 80kN and 90kN during the plasticization of the material. Finally, the cracks were forming around 12mm and propagating at approximately 15mm corresponding to the non linear phase of the specimen.

The ultimate load capacity reached for the monotonic test was almost 90kN. The ultimate load capacity calculated during the numerical campaign will have to match this value.

3.3 Qualitative description of the cyclic response of the plate

3.3.1 Global cyclic response

As a first observation of Figure 42 and Figure 43, the specimens subjected to a cyclic load had the same behaviour as during the monotonic procedure. The first part of the graph shows an elastic response until 2.5mm then a second linear behaviour characterizes the hardening process and finally a third part from 12 to 20mm describes nonlinear behaviour.

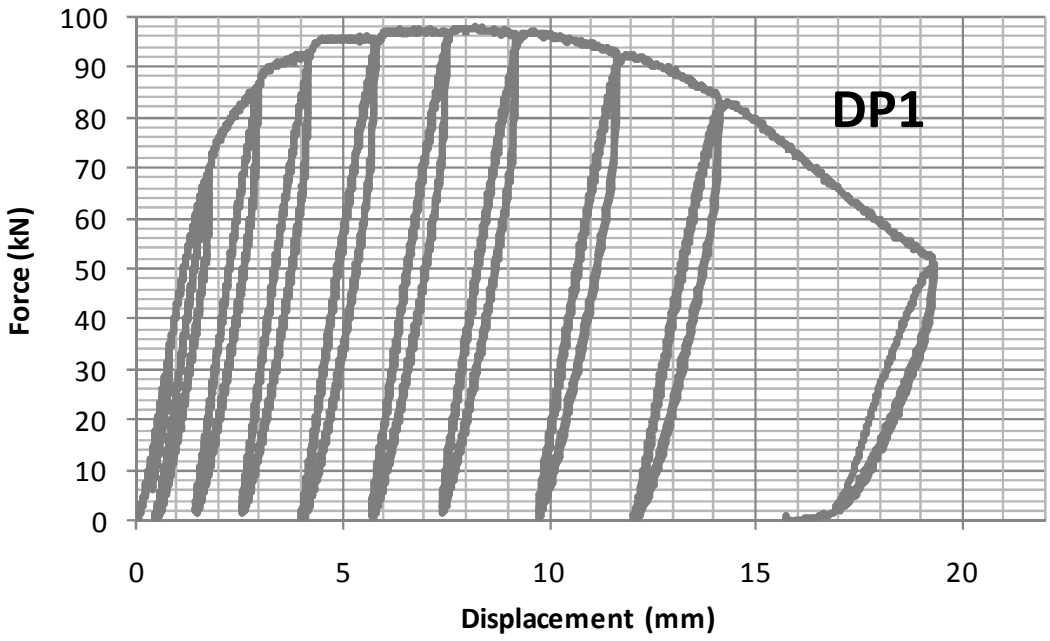

Figure 42 Force-displacement relationship of the plate DP1 under a cyclic load

Moreover, the specimen does not fully recover the residual displacements during the unloading phase which could be a problem depending on the strength and duration of the seismic excitation.

From a qualitative point of view, it is hard to discuss the different stiffness apart from the fact that the reloading phases are always characterized with a linear slope similar to the initial stiffness. The stiffness degradation will be more deeply studied in section 3.5.

Finally, it can be seen that the specimen dissipates energy creating stable loops on the force-displacement relationship once the elastic range is over. On the other hand, the area doesn't seem

very important which could mean that the anchor plate is not as effective as required. This parameter will be analysed during the numerical campaign because it is one of the main conclusions expected in this study.

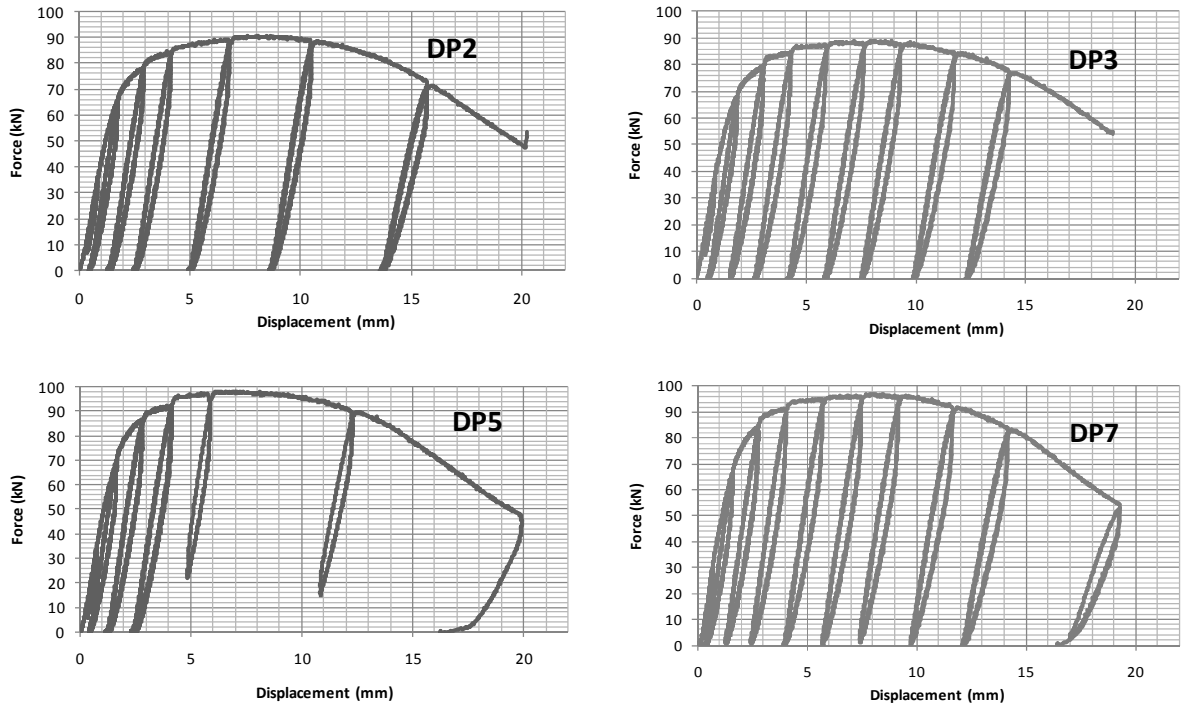

Figure 43 Cyclic response of the plate DP2, DP3, DP5 and DP7

3.3.2 Discussion on the provenance of the energy dissipation

As observed in Figure 44, the loops seem to be formed of three linear slopes which create a triangle representing the dissipated energy during the cycle by the connection. The first, which corresponds to the loading phase, is totally linear so it does not contribute to the dissipation of energy. The second, assimilated to the long part of the unloading phase, is characterized by a slight curve which contributes to the dissipation. Finally, the third corresponds to a drop of in force for a very small displacement. This phenomenon, observed in each cycle and in both elastic and plastic range at the moment of unloading, is important because it is the part of the loop which contributes most to the energy dissipation of the system. Moreover, it seems that the higher the force applied, the larger the drop.

This phenomenon is extremely difficult to justify from the results obtained and there could be many different reasons. One of the most probable factors is the friction between the plate and the base. This can be explained by the fact that the size of the gap is important if the load applied is high, which is similar to the friction definition which says the more normal force is important, the higher will be the frictional resultant force. So when the applied force is high, the friction is important and as a consequence, the plate cannot come back to its initial position until the normal force has decreased.

If this assumption is right, a discussion could take into consideration the roughness of the supporting base and the speed of the test which will affect the friction between both elements.

Furthermore, the imposed displacement to the plate has no influence on the size of the force drop, so material and geometrical non-linearity are not likely to explain this phenomenon.

This phenomenon will be compared with the numerical results in order to confirm the assumptions made.

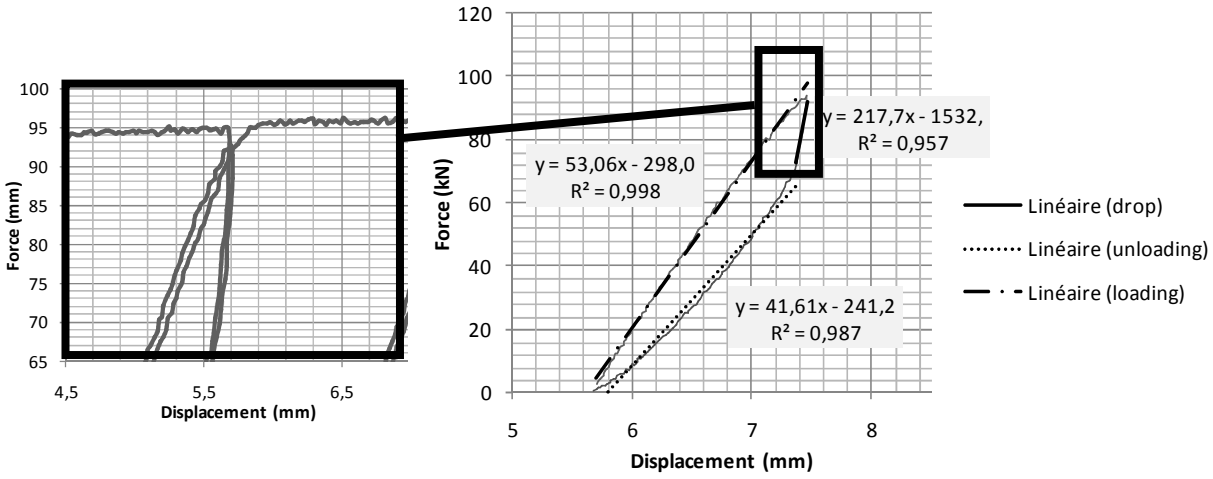

Figure 44 Study of the drop of force (left: zoom on the drop, right: trend lines of the three behaviours)

3.4 Envelope curves

Another interesting result in order to match the numerical model with the experimental tests is to plot the envelope curves of the graphs representing force versus displacement. Moreover, these two curves will give a more accurate range for the ultimate load capacity.

For this purpose, the average curves of the three vertical displacements measured on each plate were plotted against their equivalent forces. Then the maximum and minimum envelope curves of all tests were marked as shown in Figure 45

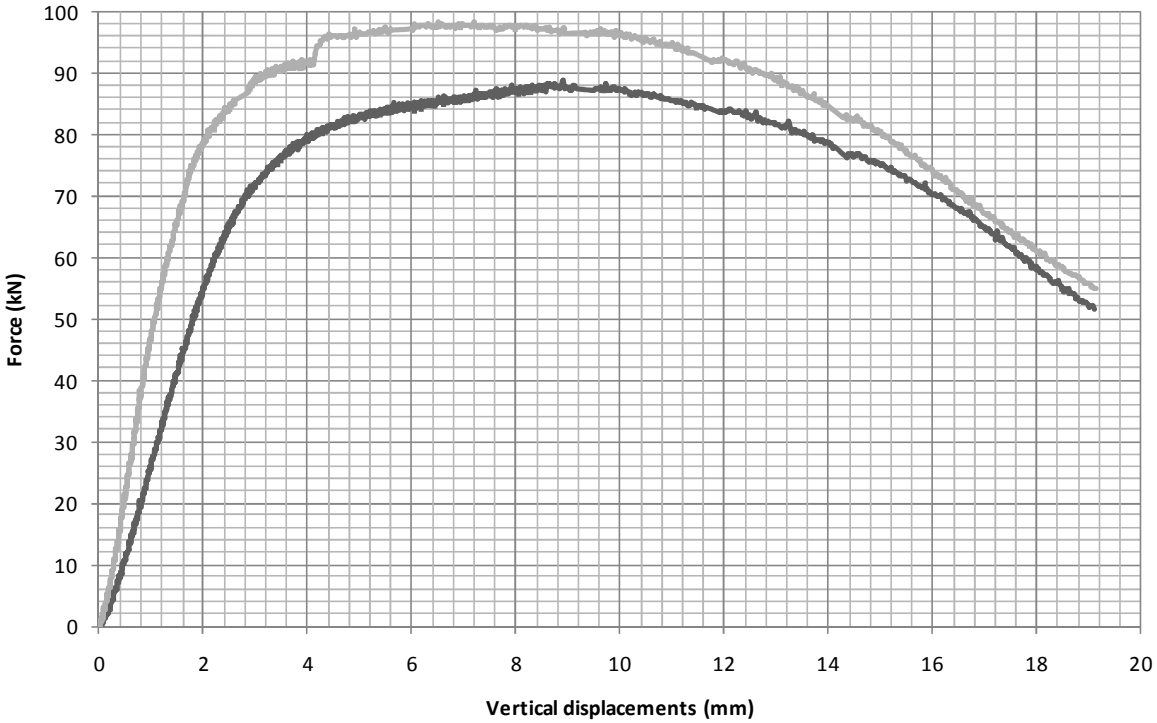

Figure 45 Envelope curves of all graphs Force versus Displacement

According to this chart the ultimate load capacity of the specimen goes from 88kN to 98kN which gives a range of 10kN. This difference is quite important since it corresponds to almost 10% of the ultimate load. The geometry summary in annex X shows that this cannot be the reason for such a difference since all the specimens had the same dimensions in a range of 2%. On the other hand, knowing that the plates were moulded, some material irregularities could increase the number of crack formations and, as a consequence, be a possible reason for such a difference in the ultimate load capacity.

During the calibration of the numerical model, these envelope curves will be an important comparison parameter. The graph relating force versus displacement from the numerical analysis will have to fit between the two envelope curves in order to confirm that the model is behaving similarly to the real plate.

3.5 Stiffness degradation

One of the main objectives of this dissertation is to understand the seismic response of this ductile anchor plate. For this purpose, the specimens were subjected to cyclic loads and this sub-chapter focuses on the stiffness degradation of the plates. This behaviour will have to be compared with the numerical results in the following chapter.

The stiffness degradations of the plates were determined by using the charts relating force against displacement from the cyclic tests shown in Figure 46. Only the graph showing the cyclic response of the plate DP7 is presented here, the rest of the graphs can be found in annex 3.

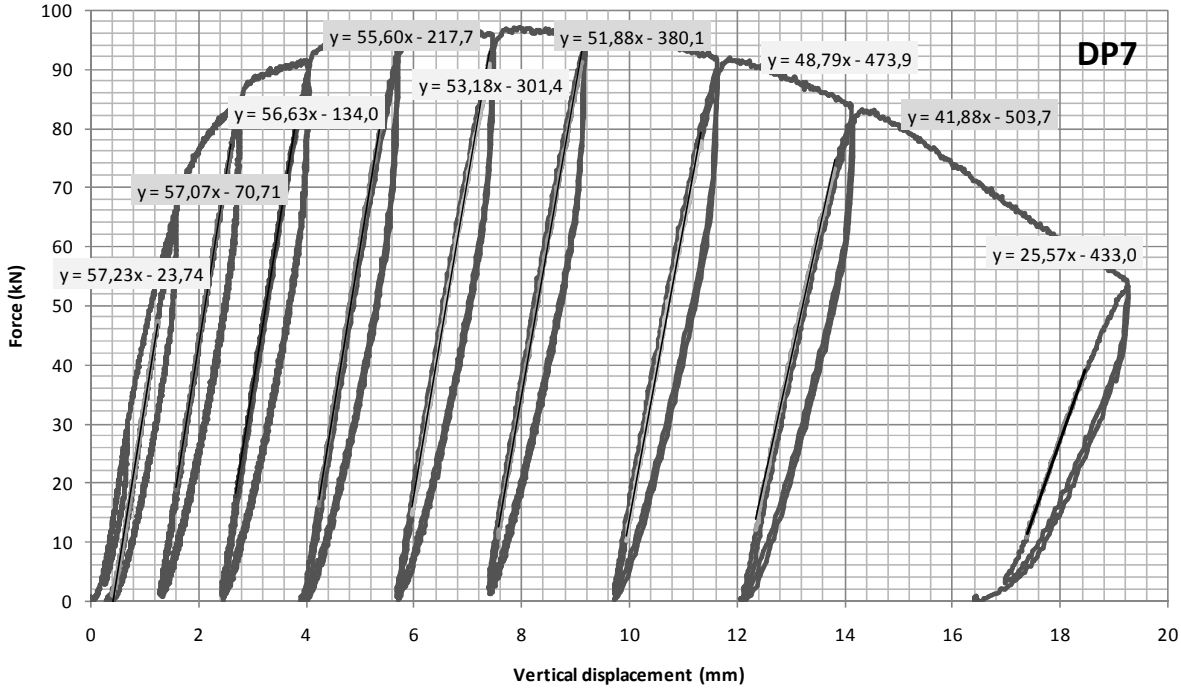

Figure 46 Slopes of the trend lines corresponding to the loading stiffness

For each cycle, the slopes of the curves representing the loading phases were computed from a trend line in Excel. The slope is a force divided by a displacement (kN/mm) which corresponds to the stiffness of the specimen during the reloading procedure. All the stiffness were summarized in Table 1 and averages and the standard deviations were calculated. Only four tests were taken into consideration in order to get more accurate results. The standard deviations calculated show that the stiffness are close which means that the retained test are consistent.

Plates	Cycles								
	1	2	3	4	5	6	7	8	9
DP1	57.15	56.15	56.67	52.82	51.61	50.15	47.82	41.22	23.47
DP2	55.95	54.41	54.3	53.05	/	50.92	/	38.27	/
DP3	55.39	54.23	53.51	52.5	49.87	49.58	46.96	41.91	/
DP7	57.23	57.07	56.63	55.61	53.19	51.89	48.79	41.88	25.57
Mean stiffness (kN.mm)	56.43	55.47	55.28	53.50	51.56	50.64	47.86	40.82	24.52
Standard deviation	0.91	1.38	1.62	1.43	1.66	1.00	0.92	1.73	1.48
Stiffness degradation (%)	0%	2%	2%	5%	9%	10%	15%	28%	57%
Displacement reached (mm)	1.30	2.85	4.00	5.50	7.50	9.20	11.40	13.85	18.80

Table 1 Summary of stiffness with average and standard deviation

Finally, the percentage of degradation was plotted against the displacement reached during each cycle in order to visualise the stiffness degradation. It can be clearly seen on Figure 47 that the stiffness of the plate decreases more severely after 12mm which corresponds to the non linear behaviour of the plate. This range is also characterized by a strong drop in the load capacity and to the first crack formation.

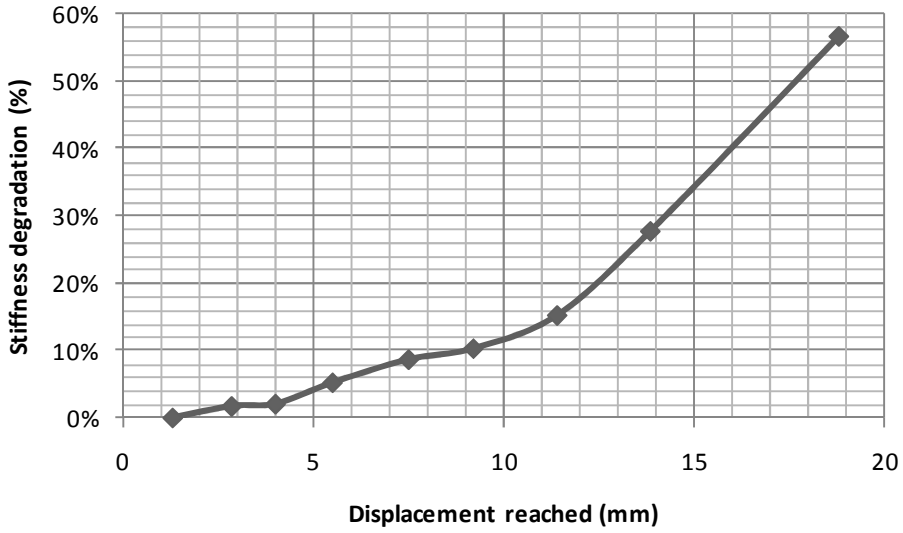

Figure 47 Stiffness degradation related to the displacement reached for each cycle

4 CONCLUSION

During this experimental campaign the specimens were subjected to monotonic and cyclic tests in order to study the seismic response of the anchor plate.

The envelope curves were plotted and the ultimate load capacity of the connection was found in between 88 and 98kN. The loading stiffness degradation was also analyzed and it was found that the decrease of stiffness corresponding to a higher displacement applied matches the global behaviour of the plate. In other words, both the load capacity and the loading stiffness start to decrease around 12mm, displacement for which micro cracks start to propagate in the end of the notches.

The results obtained in this chapter will serve as a bench mark for the calibration of the numerical model in order to be as close as possible to reality.

CHAPTER 6: CALIBRATION OF THE NUMERICAL MODEL

1 CALIBRATION PROCESS

From a modelling point of view, both the deformed shape of the plate and the data measured and analysed during the experimental campaign will be taken into account during the calibration of the model. To compare both results, the numerical ones will be plotted on the envelope curves presented in Chapter 4. All the parameters discussed in the chapter presenting the model can have an influence on the matching of the experimental and numerical results.

The geometry of the drawings has already been compared with the dimensions measured on the real plate so this parameter can be excluded. Furthermore, the mesh passed the quality software test and the geometry will not change so the modification of this parameter will not influence the results in a positive way. On the other hand, the boundary condition will affect the results as will the properties of the material. The analysis type will also be reviewed.

1.1 Boundary conditions calibration

1.1.1 Aim of the calibration of the boundary conditions

The boundary conditions were the first parameter to be updated. By comparing the deformed plate with the model, it was evident that the supports did not fully represent the reality. One of the conclusions of the experimental campaign was that while the plate was being squeezed, the supports were quickly changing from a line to points corresponding to the corners of the six petals of the plate. This phenomenon was confirmed in Figure 39 (in Chapter 5).

The aims of this part of the calibration were to allow the bottom of the plate to slide onto a base and at the same time restrict the downward vertical displacement and release the upward one. This would permit the plate to change its contact areas. To tackle this problem, several models were built by means of different elements such as interfaces or contact elements, but only one was able to run correctly.

1.1.2 Supports modelled with contact elements

The first trial was to model contact elements on both the bottom of the plate and the fixed base. Knowing that these elements often induce problems of calculation, only the expected zones were modelled with these elements in order to reduce the calculation demand. The contact elements were implemented during the mesh as eight nodded quadrilateral CQ24C elements [29] to the surfaces expected to be in contact during the analysis as shown in Figure 48. Then different properties were attached to them, depending whether they were considered as “target” or “contacter”. The contacters

were not characterized by any information but the targets were defined by parameters such as penetration depth, contact distance or friction coefficient. To model these kinds of elements, attention had to be paid to details like the normal direction of the target surfaces, or the size of the contacter that had to be smaller than the target ones.

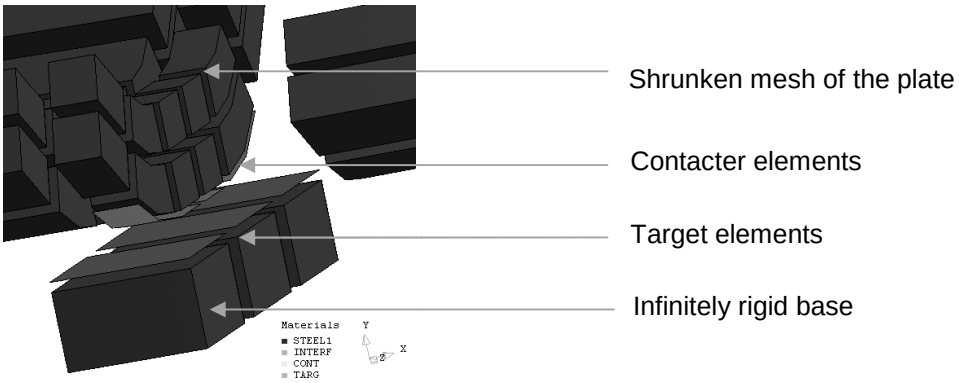

Figure 48 Detail of the expected contact area modelled with contact elements.

But despite being meticulous and rigorous during modelling, the FEM software Diana was unable to obtain the phenomenon and as a consequence all the analyses attempted were discontinued due to divergence of the solution or no convergence of the solution after 100 iterations. These calculation problems might have been caused by the curved geometry of the plate which at the same time slides and rotates inducing very complex solutions.

1.1.3 Supports modelled with interface elements

A second attempt was made by this time modelling the contact area with interfaces between the bottom surface of the anchor and a fixed rigid base. In order to have less interface areas that could lead to calculation problems, only the expected zones were modelled. As for the top ring, the interface elements were modelled by mean of bodies meshed as CQ48I plane quadrilaterals 8+8 nodded linking the plate and the base [29]. Then the base was moved to the plate so that the interface elements had no thickness as it can be seen in Figure 49. Regarding their properties, two different behaviours were tested. The first was a friction model with a linear stiffness for the resistance and non-linearity defined with a friction coulomb for the sliding concept. The second consisted in applying the same properties as for the top ring interfaces, previously detailed in Chapter 4, by means of a non-linear elasticity.

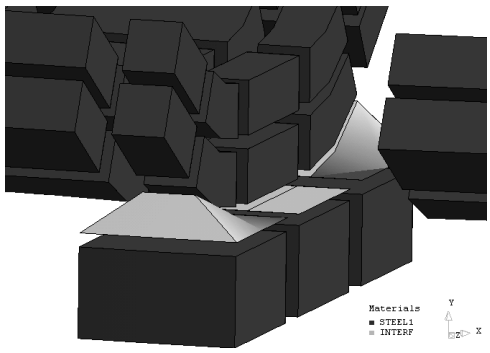

Figure 49 Detail of the expected contact area modelled with interface elements.

For this model, the problem was that the plate was going through the interfaces without being restrained leading to useless supports. This phenomenon can be explained by the fact that since the contact area is rotating, the interface element modelled between the fixed base and the plate is subjected to compression and tension at the same time so the element is just releasing all nodes.

1.1.4 Supports modelled with simple vertical supports

The last available solution was to keep the simple vertical support as for the preliminary model with the difference being that only the corners were fixed instead of a whole line, as presented in Figure 50. The experimental campaign showed that the plate was only supported on the sides of the petals so fixing one node on each side was at least more realistic than the preliminary model. Thanks to the simple vertical supports, the analysis was able to run without any problems since the calculations were much easier. On the other hand, the model was closer to reality than the preliminary one but not fully describing the real response. Since there were no other possibilities, this solution was retained. In terms of results, even if this option wasn't the most desired of the contact techniques, the improvement of the behaviour was noticeable as will be observed in the following Sections.

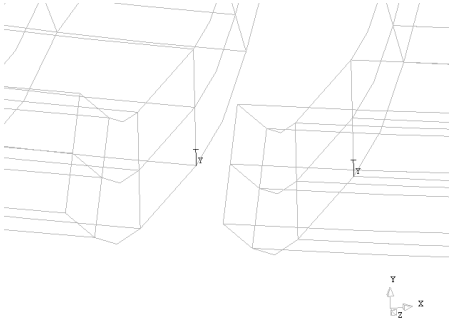

Figure 50 View of the final boundary conditions.

1.2 Analysis type calibration

A decrease in the ultimate load was observed in the previous part but this load capacity and the behaviour of the model were still far from the experimental ones. The numerical curve presented in Figure 51 showed that when the plate was starting to deform plastically, leading to larger

deformations, behaviour was not affected and the equivalent forces remained constant. The reason found for this problem was that only the material non linearity was taken into account. According to [15], if the ratio of a structure deformation and its largest dimension is greater than 1/20th, a geometrically non-linear analysis should be used. In our case, the ration of the largest deformation (20 mm) and largest dimension (250 mm) is greater than 0,05 so this type of analysis was added in the procedure by mean of the Total Lagrange (TL) method. This type of analysis improved the results but the curve still did not match the envelopes so the Updated Lagrange (UL) method was used to characterize the geometrical nonlinearity of the model. The UL analysis, as opposed to the TL method, uses an updated reference geometry. To its advantage, the UL analysis correctly describes large displacements, rotations and strain, but this method is extremely expensive in terms of calculations and as a consequence much more time consuming than the TL analysis. The improvements of results made by changing the analysis type can be observed in Figure 51. The results obtained from this calibration still did not perfectly match the experimental envelopes but the shape of the curve was now quite similar to them.

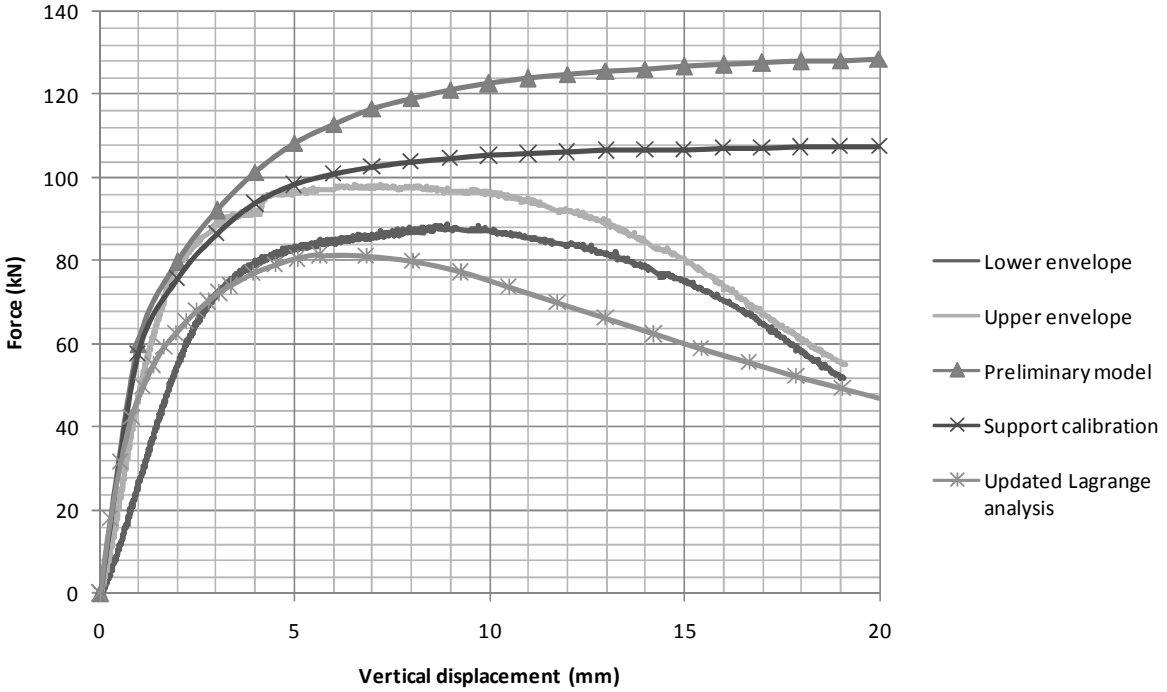

Figure 51 Evolution of the model behaviour during the first calibration steps.

1.3 Material properties calibration

All the other characteristics of the model being implemented as close as possible to reality, the last parameters to be calibrated were the material properties.

1.3.1 Interface elements

First of all the interface element properties defined in Chapter 4 were reviewed. The normal stiffness was kept infinite but the tangential stiffness was lowered to a very low value in order to disconnect the ring and the plate. This could be understood as modelling a contact with almost no friction.

1.3.2 Steel

1.3.2.1 Selection of the variables influencing the parametric study

Regarding the steel, it was defined during the preliminary modelling by a Young modulus of 210 GPa, a Poisson ratio equal to 0.3, a yield strength at 0.2% of deformation of 210 MPa, and an ultimate strength equal to 505 MPa [30]. With these properties, the model response still did not coincide with the experimental results so a parametrical study was carried out to find the appropriate characteristics to attach to the steel elements.

In order to avoid a too time consuming parametric study, some parameters had to be fixed. Firstly, it was observed that the initial stiffness was slightly higher than the experimental value, so the Young modulus was lowered to 170 GPa, which didn't much affect the curve shape. Moreover, the Poisson ratio seemed reasonable so it was kept equal to 0.3, which left only the yield strength and the ultimate strength to be calibrated.

But as can be seen on the stress - equivalent plastic strains diagram implemented in Diana (Figure 54), the yield strength is given for 0% of strain and the ultimate strength coordinates depends on two values (stress and strain), which led to three unknowns. In order to simplify this study, the plastic strain corresponding to the ultimate load was fixed at 0.6%. Knowing that strains are one of the first variables to be calculated in FEM, the definition of this parameter is important and could be calibrated through a sensitivity analysis run in tandem with a uncertainty analysis.

1.3.2.2 Parametric study

From there, three different values were chosen for both the yield strength (150 MPa, 250 MPa and 350 MPa) and the ultimate strength (400 MPa, 500 MPa and 600 MPa), then a last intermediate value was defined for each parameter depending on the first results obtained. In total, sixteen analyses were calculated by changing only one parameter for each of them.

The parametric study was carried out with two parallel methods. The first, shown on Figure 52, was purely graphical and consisted in observing the matching of the numerical curve with the experimental envelopes. The second, more numerical, was based on (5); relating the two parameters to be calibrated with an objective function (π) of three calculated relative errors. As a consequence, the lowest will be π, the closest will be the model from the experiments.

$$\pi = \frac{1}{2} \times \left(\sum_{i=1}^{3} \text{Error}_i \right)^2 \quad (5)$$

Error 1 was comparing the difference between the ultimate load capacity of the model and the mean value from both envelope curves, Error 2 was characterising the difference between the displacements corresponding to this ultimate load and Error 3 was describing the difference between the forces corresponding to a displacement of 16.5 mm. Finally, each relative error was weighted regarding its importance (W_1=0.6, W_2=0.3 and W_3=0.5) in the matching of the results and the function was plotted as a surface in Figure 53.

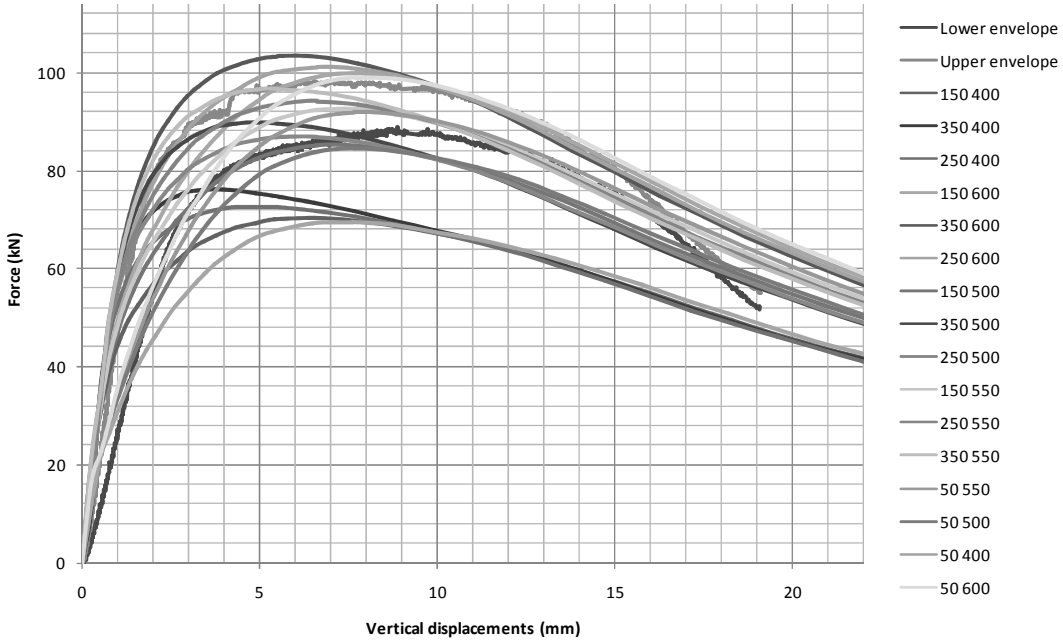

Figure 52 First parametric method analysing the fitting of the numerical results in the experimental envelope.

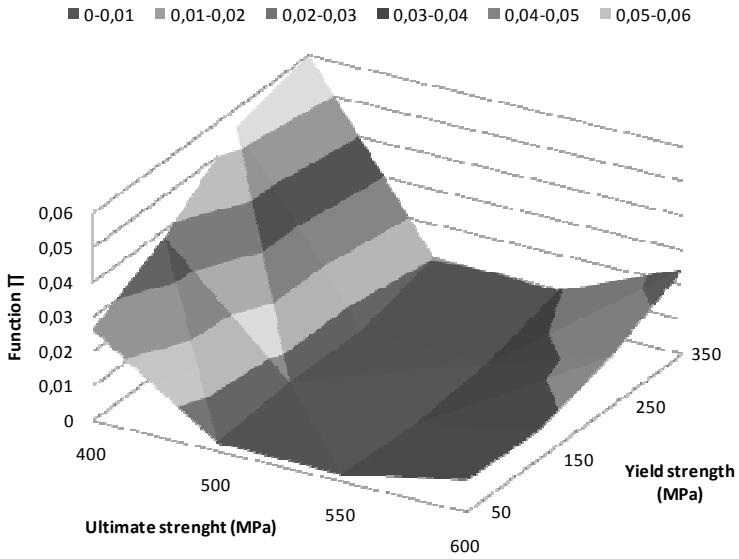

Figure 53 Second parametric method linking relative errors between numerical and experimental results with variables of the parametric study.

1.3.2.3 Conclusion of the parametric study

In conclusion of the material calibration process explained above, the final steel properties attached to the model were characterized by a young modulus of 170 GPa, a yield strength equal to 150 MPa and an ultimate strength of 550 MPa, corresponding to a plastic strain equal to 0,6%. The constitutive law of the implemented steel is described in Figure 54 showing the stress - equivalent plastic strains relationship. The superposition of the experimental envelopes and the numerical curve calculated with the final steel properties is presented in Figure 62.

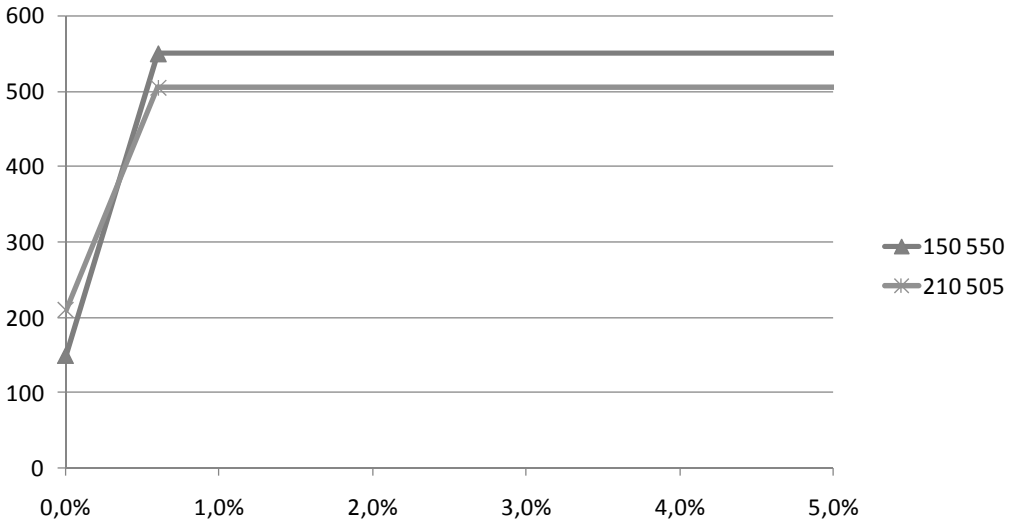

Figure 54 Stress - equivalent plastic strains relationship.

As explained in Chapter 4, a coupon tensile test would have been much more accurate and would have led to a better calibration of the steel properties and consequently of the model but for time reasons this could not be possible.

2 FINAL RESULTS OF THE NUMERICAL MODEL

2.1 Principal stresses

The principal stresses are the stresses given for a plane in which the tension vector has the same direction as the normal vector so the total tension is equal to the normal stress. In other words, these stresses show whether the element is in traction (principal stress 1) or in compression (principal stress 3) and thus give us a general idea of the behaviour of the plate. The high tensile stresses can clearly be observed at the end of the openings which tries to open and at the bottom surface of the top of the plate which is tensed when the plate is squeezed.

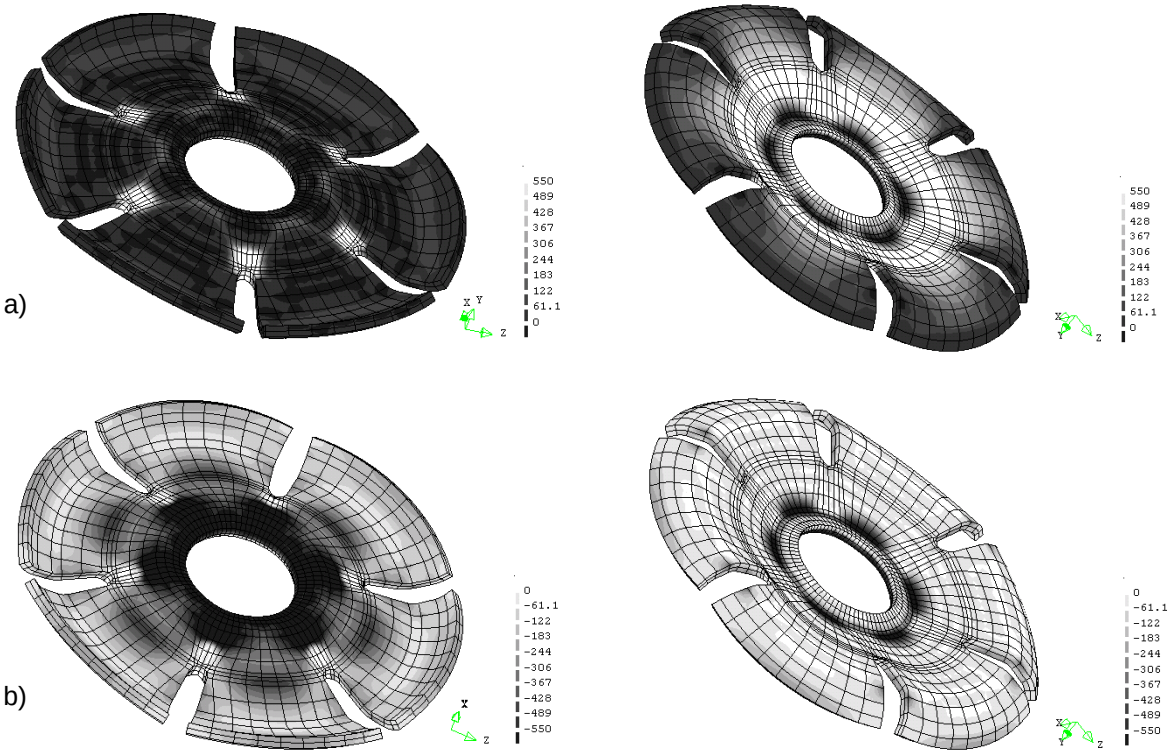

Figure 55 Principal stresses on deformed shape with magnification factor equal to 1: a) Top and bottom view of P1 plotted from 0 to 550 MPa; and b) Top and bottom view of P3 plotted from -550 MPa to 0.

2.2 Von Mises stresses

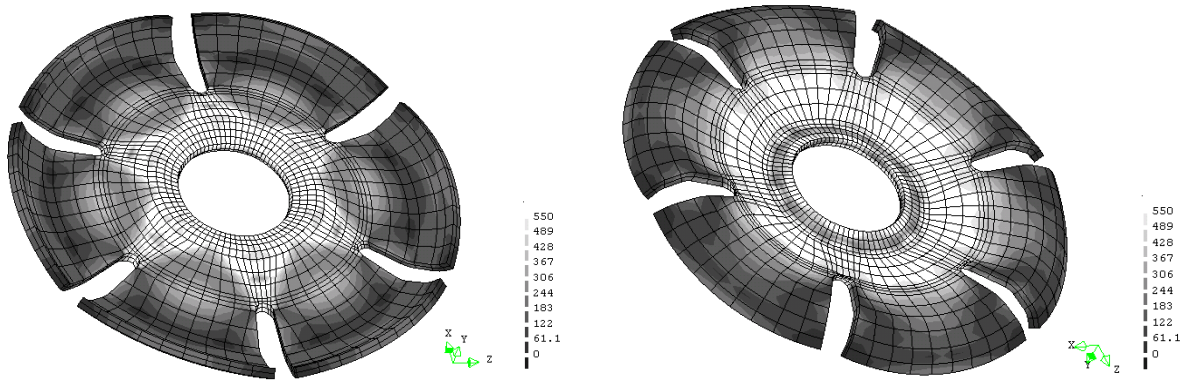

Figure 56 Von misses stresses plotted from 0 to 550 MPa on deformed shape with magnification factor equal to 1 (top and bottom view).

The Von Mises model was implemented in the software Diana as the failure method governing steel. In this way, all stresses higher than the ultimate strength of 550 MPa calibrated previously show a yielding process of the steel. As can be seen on Figure 56, the openings and the top part of the plate present a high level of stress whereas the petals undergo almost no yielding. This confirms the

assumption made on the global behaviour that the plate tended to separate into 6 petals linked on the top of the ring. As a consequence, when the plate is squeezed all the petals try to open by creating cracks in the openings and thus no flexural behaviour is observed on the plate.

2.3 Ultimate load

In terms of capacity, the model attains an ultimate load of 92.5 kN for a displacement of 7.7 mm. The monotonic response of the model is described in Figure 62.

2.4 Stiffness degradation

The global cyclic response of the model can be observed in Figure 57. As for the experimental results, an interesting parameter to be calculated regarding the cyclic behaviour of the model was the stiffness degradation occurring after each cycle. For this purpose, the slope of the curve was calculated by means of a trend line for each cycle in order to calculate the stiffness of each of the reloading phases. All the slopes as well as the stiffness degradation expressed in percentage are summarized in Table 2, which demonstrates that at the end of the test, the plate lost 75% of its initial stiffness.

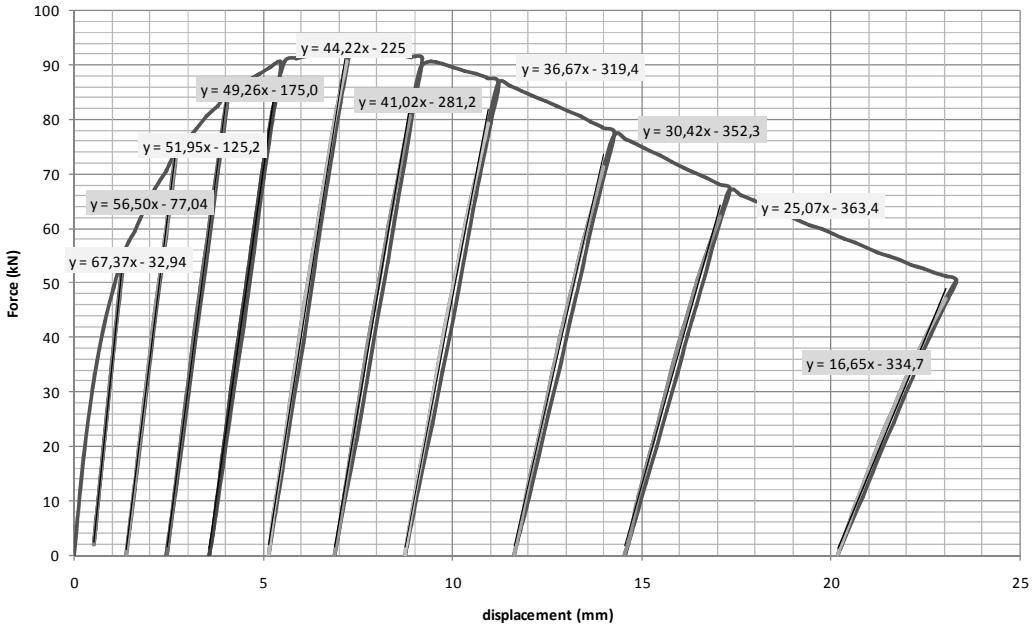

Figure 57 Stiffness degradation during numerical cyclic test.

	Cycles									
	1	2	3	4	5	6	7	8	9	10
Stiffness (kN.mm)	67.4	56.5	51.9	49.3	44.2	41	36.7	30.4	25.1	16.7
Stiffness degradation	0%	16%	23%	27%	34%	39%	46%	55%	63%	75%
Displacement reached (mm)	1.3	2.7	4	5.3	7.2	8.9	10.9	14	17.1	23

Table 2 Summary of stiffness degradation expressed in percentage.

3 COMPARISON OF NUMERICAL AND EXPERIMENTAL RESULTS

This paragraph aims to assess the correspondence between the numerical and the experimental results and to present the accuracy of the analogy made out of both models.

3.1 Comparison of the final deformed shape

The two global deformed shapes match quite well even if the appearance is affected by the perspective issues. When the plate deforms both of the specimens open the petals creating a kind of arch above the support and presenting some waves on top of the plate. But a difference can be observed on top of the plate by paying attention to the outline of the inner hole which undergoes a larger deformation in the model than in the experiments. The reason for this could be that the interface created between the ring applying the load and the top of the plate doesn't act as a perfect contact surface.

a) b)

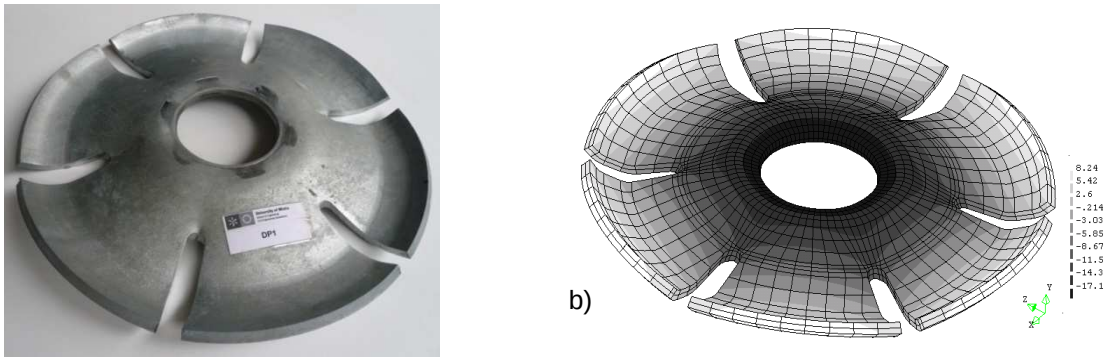

Figure 58 Comparison of deformed shapes: a) Experimental deformed shape; and b) Numerical deformed shape with vertical displacements.

3.2 Correspondence between observed damages and calculated stresses

As a qualitative approach, the comparison of the stress distribution on the model and the location of damage on the tested specimen provide interesting information about the correspondence between the prototype and the model. In order to better understand the overall behaviour, the stresses were plotted on the deformed shape.

3.2.1 Location of cracks

According to Figure 59, the correspondence is evident between the cracks that appeared during the experimental campaign and the concentration of high principal stresses describing a tensed area (white elements) and thus predicting cracks. Unfortunately, the software Diana doesn't offer the possibility to implement a crack model for a steel material so the cracks cannot be seen in the numerical model.

a)  b) 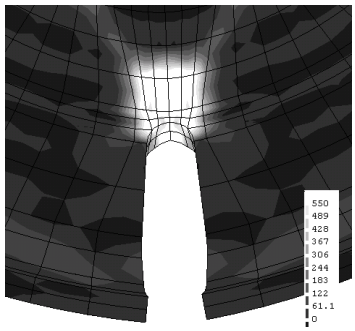

Figure 59 Comparison of crack location; a) Experimental crack in opening, and b) Principal stresses P1 in opening.

3.2.2 Crushed sides of petals

During the experiments, it was observed that the boundary conditions were changing to a punctual support and thus the sides of the petals were crushed at the end of the tests. It can be seen on Figure 60 that the stress distribution of the principal stresses P3 representing the compression state do not even reach the ultimate strength which means that this phenomenon is not well described on the model. The most probable explanation is that the crushing of the material during the test was due to the sliding of the supports, in other words the friction between the plate and the base which hasn't been modelled in this way as explained in chapter 4.

a) 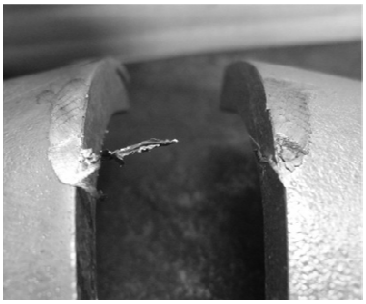 b) 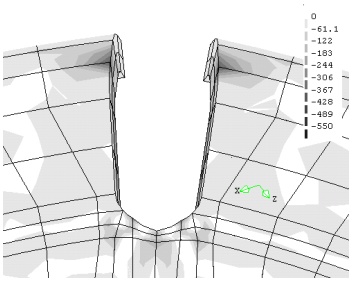

Figure 60 Comparison of support: a) Experimental crushed support; and b) Principal stresses P3 on modelled support.

3.2.3 Waves on top of the plate

The wave shaped deformation of the top of the plate observed during the experimental campaign (see Figure 61a) can be explained thanks to the numerical model. When the plate is squeezed the top outline of the hole is totally in compression (see Figure 61b) and wants to deform but the resistance in the plane of the hole is much higher than the resistance of the section corresponding to the thickness of the plate. As a consequence, the top of the plate deforms in the plane of the weakest resisting section which means that the top of the plate buckles. Moreover, the different points where the top ring buckles are governed by the position of the openings make these areas weaker. This phenomenon

can be seen in Figure 61c and 14d which respectively show the concentration of high compressive and tensile stresses on the high point and lower point of the waves on the bottom surface of the plate.

a)

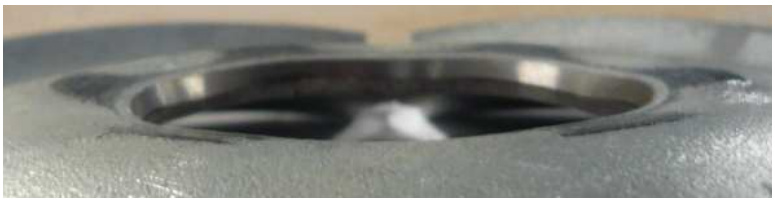

b)

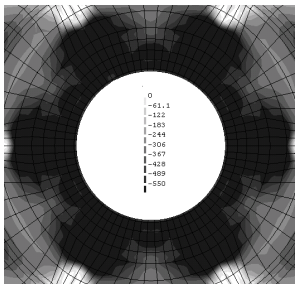

c)

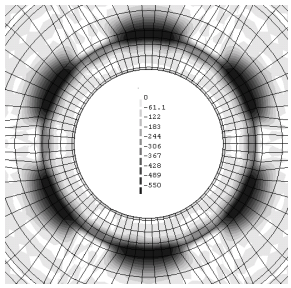

d)

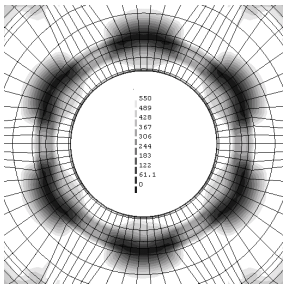

Figure 61 Comparison of the top of the plate: a) Experimental deformed shape; b) Principal stresses P3 top view of the hole; c) Principal stresses P3 bottom view; and d) Principal stresses P1 bottom view.

3.3 Global response of the plate under monotonic load

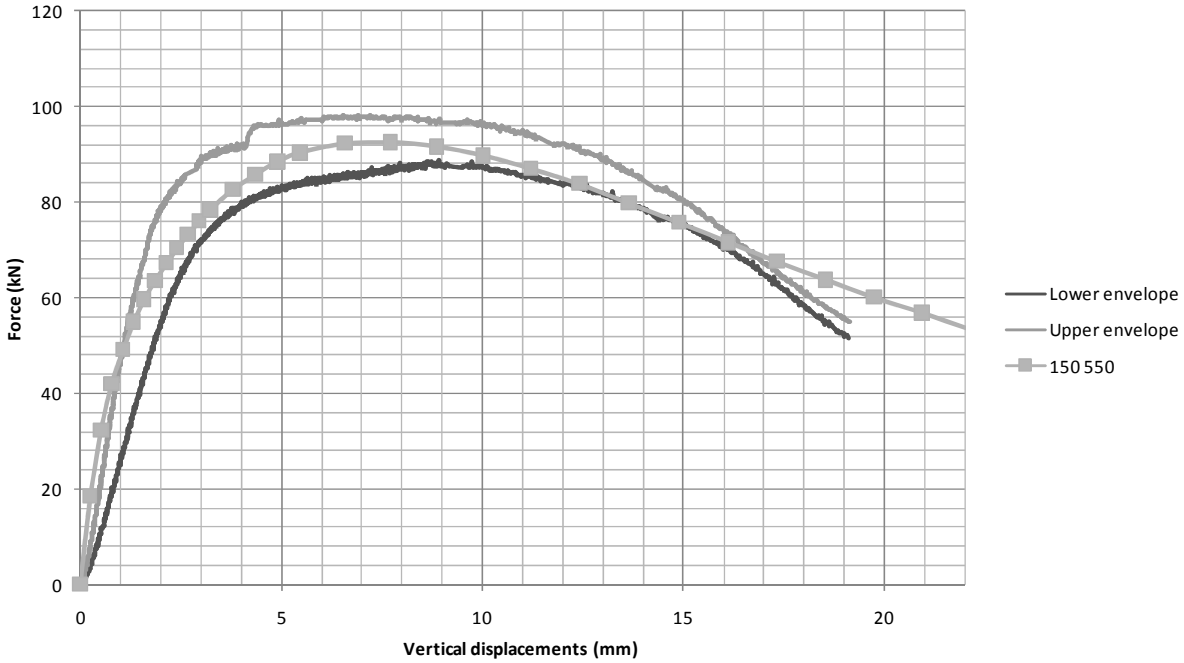

Figure 62 Comparison of the numerical and experimental response under monotonic load

The force-displacement relationship characterizing the plate response was the base of the calibration so as a consequence the experimental and numerical results are quite similar and the calculated

curve fits the measured envelope curves well. The ultimate load and the equivalent displacement for this peak of both campaigns match very well a relative error equal to respectively 0.53% and 0.52%, which is not a surprise since these two parameters were the base of the model calibration. Moreover, the initial slope and the global shape of the numerical curve are also pretty close to the experimental ones as can be observed in Figure 62. However, the last part of the chart shows that the model does not perfectly reflect the tested specimen taking into consideration that the last non-linear behaviour of both numerical and experimental methods does not superpose well.

3.4 Global response of the plate under cyclic load

3.4.1 Overall discussion on the global response

In order to have a global idea of the difference between the numerical and experimental behaviour of the plate under a cyclic loading, the numerical results were plotted with the results obtained from the specimen DP1 and with the envelopes of the experimental campaign (Figure 63). In terms of the envelope, the numerical curve has the same behaviour as the curve corresponding to the monotonic loading presented in the previous paragraph. Regarding the cycles, the curve is similar to the experimental one from the point of view of residual displacement after the unloading phase. Moreover, the stiffness is also comparable and undergoes a stiffness degradation which will be discussed in the following paragraph. But, by paying attention to the loop formed by the cycles, it can be observed that the numerical ones are almost nonexistent which means that almost no energy is dissipated through the cycle. This last parameter will be studied in the last paragraph.

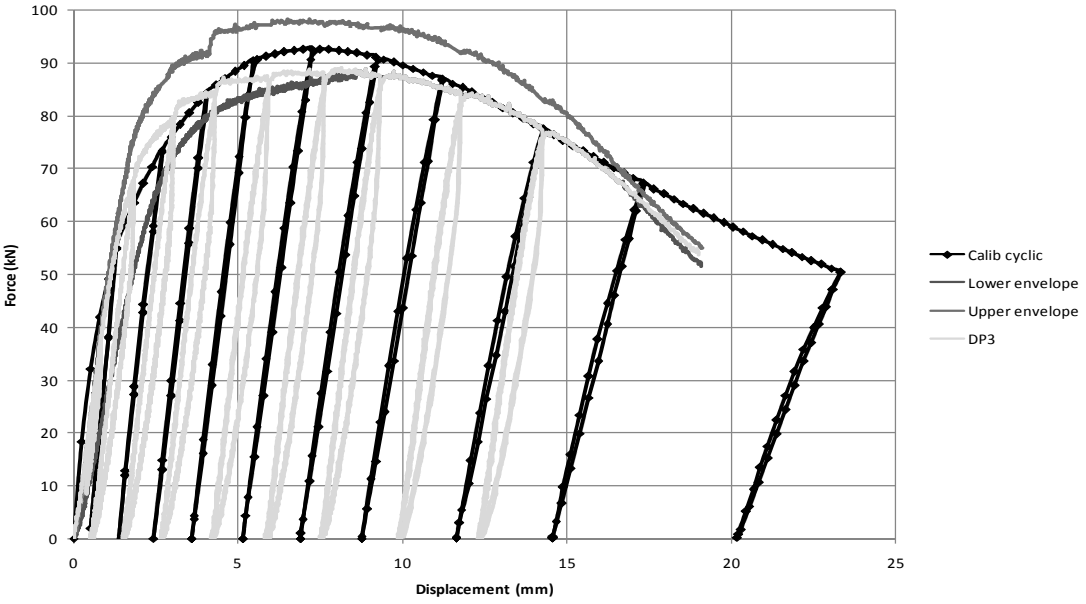

Figure 63 Numerical and experimental response of the plate under cyclic loading

3.4.2 Comparison of the stiffness degradation

For both the numerical and the experimental campaign, the stiffness of the loading phase was calculated for each cycle. From these values, it was possible to determine the stiffness degradation percentage occurring cycle after cycle. Finally the stiffness degradation was plotted against the respective displacement of each cycle as presented in Figure 64. It is interesting to observe that the numerical model undergoes a drop of 15% of its stiffness and then decreases linearly, whereas the experimental results show that the stiffness degradation seems to increase in an exponential way.

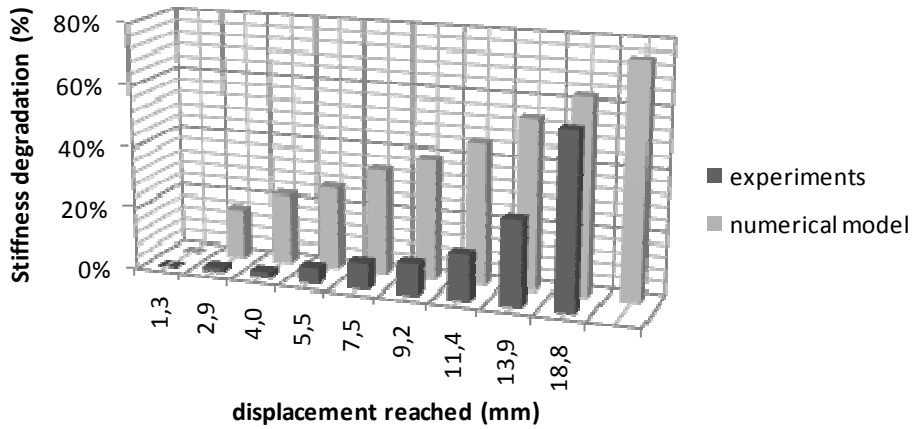

Figure 64 Comparison of the numerical and experimental stiffness degradation

3.4.3 Comparison of the dissipated energy

It was observed during the analysis of the experimental results that a force drop occurs when the unloading starts and induces a dissipation of energy by creating a loop. On the other hand, the numerical model does not show this behaviour as shown in Figure 65. The assumption made was that the force drop is induced by the friction between the plate and the supporting base.

Since the numerical model was developed without any friction because of some problems detailed in the beginning of this chapter, the assumption made during the experimental campaign seems to be confirmed. As a consequence, it can be concluded that the dissipation of the energy is provided by two parameters:

- Plasticization of the steel or non-linearity of the geometry which is very difficult to differentiate, characterized by a small curvature of the slope during the unloading phase,
- Friction phenomenon between the plate and the base creating a force drop on the force – displacement diagram and thus increasing the area of the loop.

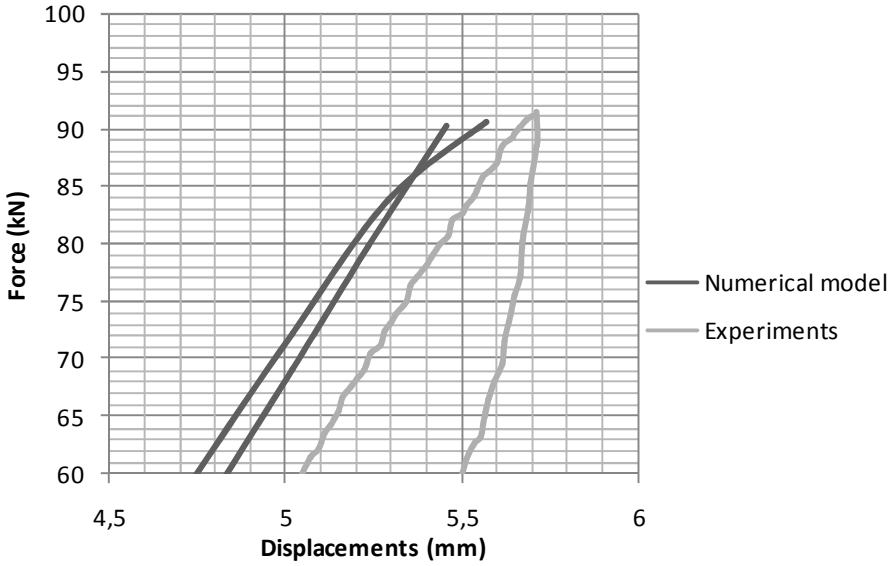

Figure 65 Comparison between the end of a numerical and experimental cycle.

4 CONCLUSION

The calibration carried out helped to improve the type of analysis, the boundary conditions and the material properties. This last parameter was determined through a parametric analysis by running sixteen analyses though it would have been more accurate to do a coupon tensile test on a steel sample.

The final numerical results provided useful information such as yielding areas as in the openings for example, or the stiffness degradation occurring during the cyclic loading. Principal stresses were also plotted to confirm the global behaviour by looking at regions in tension or compression.

Finally a comparison between both experimental and numerical results was accomplished by means of qualitative and quantitative methods. The correspondence between damages and high stress distribution was observed for the openings or for the buckling phenomenon taking place on the top of the plate. Moreover, the cyclic response of the plate was analysed and some similarities were observed such as the residual displacements after plastic deformation. On the other hand, the model was close to not recreating the dissipated energy seen during the experiments.

To conclude, the comparison of the results showed that the model was a good representation of the real plate.

CHAPTER 7: GLOBAL DISCUSSION ON THE PLATE

1 COMPARISON OF THE PLATE STIFFNESS WITH THE CONNECTED STRUCTURAL ELEMENTS

1.1 Aim of this comparison

In structural connection design, it is of great importance to study the local behaviour of each element whithin the connection system in order to predict the failure mechanism. This is even more important when considering ductile connection design in which the weakest element of the connection should be the one expected to dissipate energy so as not to affect the surrounding elements. Both the stiffness and the ultimate load of the structural elements composing the connection are of extreme importance in the design process.

In the case of the ductile plate studied in this thesis, it will be implemented on a masonry wall and anchored to a steel tie. Therefore, the stiffness of the plate will be compared to a steel tie and masonry wall stiffness. The aspired result of this comparison is to demonstrate that the stiffness of the different elements are ordered as $K_{plate} < K_{tie} < K_{wall}$ so that the plate deforms in a greater range than the other components. The other parameter to control is the ultimate load, corresponding to the elastic range of each element, in order that the wall and the tie stay in their elastic range and do not undergo large deformations leading to failure, especially the wall which is the part of the structure to be protected and demonstrates brittle behaviour.

1.2 Stiffness of the plate

The stiffness of the plate is one of the results of the study carried out in this thesis. The numerical and experimental campaign characterized the stiffness around 56 kN/m. Moreover, it was observed that the plate undergoes stiffness degradation when the imposed displacement increases, though this does not affect our comparison since the plate's stiffness has to be the weakest one.

1.3 Stiffness of the steel tie

In order to obtain a range of stiffness for steel ties, two cross sections, with for each of them two lengths and two different areas were chosen which would lead to a lower and an upper bound to be compared with the plate's stiffness. The dimensions were taken according to an experimental campaign carried out at the University of Minho, Portugal, focusing on the identification of the tensile force in tie-rods [31]. The dimensions which were studied can be found in Table 3. Moreover, knowing that during a seismic retrofitting the rods are usually replaced with new steel ties, the Young modulus was taken as equal to 210 GPa which represents a common steel grade.

The stiffness of the different ties was calculated according to (6) and is presented in Table 3 along with the dimensions of different type of steel ties. It can be observed that the range of stiffness goes

from 10 to 100 kN/mm depending on the section and the length. The stiffness of the plate is equal to 56 kN/mm so for this reason the steel tie is chosen with a slightly higher rigidity for the purpose of this comparison, equal to 70kN/mm for example.

$$k = \frac{E \times A}{L} \tag{6}$$

Cross section shape	Circular	Circular	Rectangular	Rectangular	Circular	Circular	Rectangular	Rectangular
Length (mm)	2700	2700	2700	2700	5400	5400	5400	5400
Diameter / Side (mm)	15	25	25	35	15	25	25	35
Area (mm²)	176.6	490.6	625	1225	176.6	490.6	625	1225
Young modlous E (GPa)	210	210	210	210	210	210	210	210
Stiffness (kN/mm)	13.74	38.16	48.61	95.28	6.87	19.08	24.31	47.64

Table 3 Summary of dimensions and stiffness for different type of steel ties

1.4 Stiffness of the wall

The out of plane stiffness of unreinforced masonry walls is a concept extremely difficult to characterize depending on the geometry of the wall, its structural characteristics and boundary conditions. Within the scope of this thesis, the purpose is not to study the walls so calculations were reduced to a simple analogy of a cantilevered wall. Its stiffness is thus given by (7) where E is the Young modulus, I the inertia regarding the out of pane deformation, and L the height of the wall.

$$k_{wall} = \frac{3 \times E \times \mathrm{I}}{L^3} \tag{7}$$

As an example, the height was taken as equal to 3m, the Young modulus 5 GPa and the base width 0.3 m. These values lead to a Stiffness of 135kN/mm, which is higher than the stiffness of the other elements as should be.

1.5 Comparison

The Comparison of the stiffness is based on an electrical analogy. The stiffness is compared to the inverse of the electrical resistance. The assumption made is that the system works as do resistors organized in series (see Figure 66). Thus, the total resistance, equal to the inverse of the total stiffness K_{TOT}, is equal to the sum of the resistance, as shown in (8), until one of these elements moves to a plastic range. According to this analogy, attention has to be paid to the number of plates implemented, because in parallel, the stiffness is additional and thus the global behaviour will not be ductile anymore.

$$\frac{1}{K_{TOT}} = \frac{1}{K_1} + \frac{1}{K_2} + \frac{1}{K_3} \Leftrightarrow R_1 + R_2 + R_3 = R_{TOT} \tag{8}$$

Therefore, when the three elements are connected, global stiffness decreases but on the other hand the displacements are divided in such a way that the weaker element will undergo the highest deformation. In the case treated, the global stiffness will be equal to 25 kN/mm.

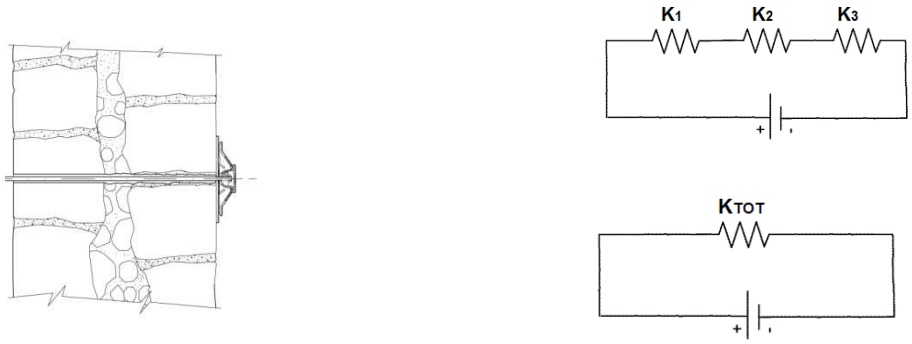

Figure 66 Electrical analogy of the ductile system

As a consequence, for example, of a global displacement of 1 mm from the earthquake, the corresponding global force subjected to the system will be 25 kN. Then, the local displacement of each element of the system is given by (9), taking into consideration the force subjected to the global system equal to 25 kN and the individual stiffness of the elements. Thus, the wall will undergo a displacement equal to 0.18 mm and the plate will deform 0.44 mm. Without the plate, the global stiffness would be higher, therefore the global force would also be higher and the wall would undergo greater deformation which could cause more damage.

$$d = \frac{F}{K} \tag{9}$$

Figure 67 gives a visual understanding of the behaviour of the ductile system. This graph can easily provide the distribution of the displacements in the system subjected to an excitation. It is important to note that this graph, and the method related to it, is only valid until the global force of the connection reaches the load corresponding to the end of the elastic range to any of the elements.

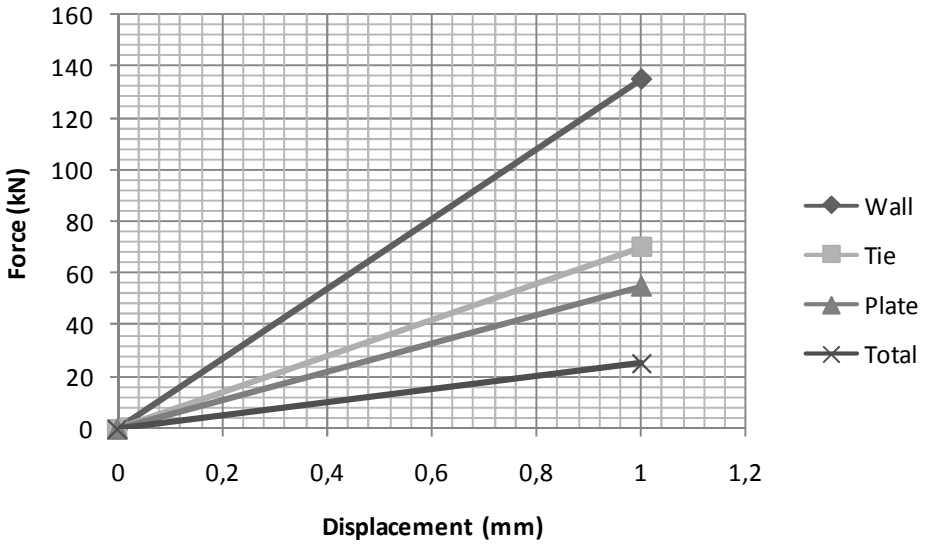

Figure 67 Force-Displacement diagram for each element and the global connection

If the ultimate load of the wall is not high enough to undergo the global force, ductility to failure could be added to it by means of reinforcement techniques such as near surface reinforcement so that the wall failure is not so brittle and can undergo larger displacements.

To conclude, this comparison is not given as quantitative comparison, but as a possible process to design several ductile connections on a building. As a consequence, the wall characteristic, which are very variable and not so realistic in this case, should be defined for each retrofitting case studied.

2 DISCUSSION ON THE SEISMIC BEHAVIOUR OF THE PLATE

2.1 Response observed

The main expectation of this plate was focusing on its capacity to dissipate energy. This process can be observed on the force–displacement diagram of the device in which loops should be created by the loading–unloading process. It was observed in both numerical and experimental results that this loop was quite small due to two similar behaviours while the plate is loaded and unloaded. Moreover, it was seen that once the plate goes out of its elastic range, it shows residual displacements. These increase proportionally to the imposed displacement which can be seen physically by the fact that the anchor does not recover its initial shape when it is unloaded. As a conclusion to these observations, the plate does not behave as expected in terms of dissipation of energy

2.2 Response expected

As explained in the previous paragraph, the two points to improve are the residual displacements and the amount of dissipated energy. This could be obtained by means of a force–displacement diagram shaped as a flag hysteresis. Figure 68 presents the ideal expected response for one cycle. The device represented by this diagram shows an important initial stiffness until it reaches its yield strength, then responds with a second stiffness inducing larger displacements. When the system is unloaded, a self-centering response is observed and allows the device to recover its displacement and thus its initial deformation. The flag corresponding to negative displacements and forces has the same explanations but is constructed when the system is subjected to traction. This does not concern our study because this would mean that the tie rod is in compression.

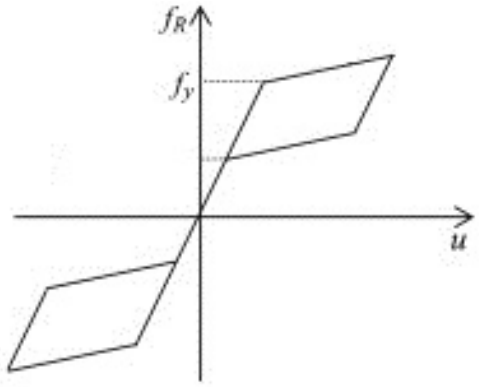

Figure 68 Expected flag hysteresis response.

2.3 Improvement of the seismic behaviour of the plate

In order to obtain a diagram as shown in Figure 68, several improvements could be made to the plate at the same time keeping the cost of the system low. For example, the first drop of force on the diagram could be obtained through a greater friction area, created here by means of additional support between the plate and the supporting base. This added support is presented in Figure 69.

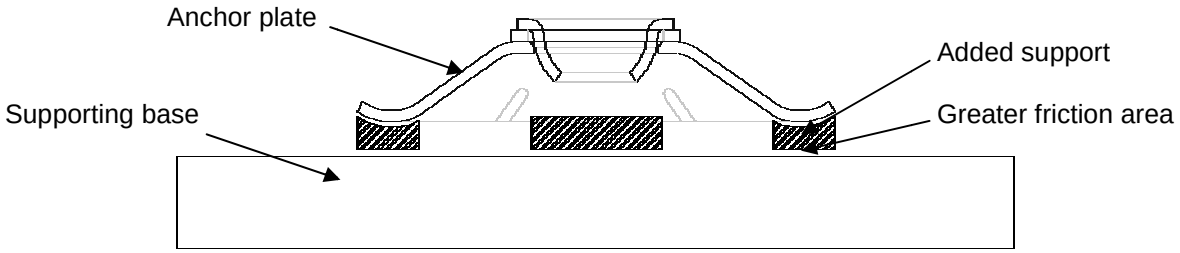

Figure 69 Proposed improvements of the ductile anchor

Once again this proposed improvement involves both contact and friction problems and thus could be problematic to implement in a numerical model. On the other hand, a greater friction process would take place between the added part and the supporting base, both coplanar, and thus the physical problem should not be too complicated to model in a FE programme. The contact between the plate and the added support could be kept as simple supports to begin with in order to show improvements made by the added devices.

Moreover, attention should be paid to the type of steel used which will influence the self-centering response by avoiding plasticity of the plate. A specific steel called “spring steel” could be used so that the yield strength is very high in order to maintain position in the elastic range of the plate. The geometry could thus be used in a more efficient way.

Another solution would be to put two plates one on top of the other (Figure 70). In this way, the friction between both plates would dissipate energy because both geometries will match perfectly and thus the contact area will be greater. In this case, the young modulus or the thickness of the plate should be reduced in order to obtain the same stiffness as only one plate.

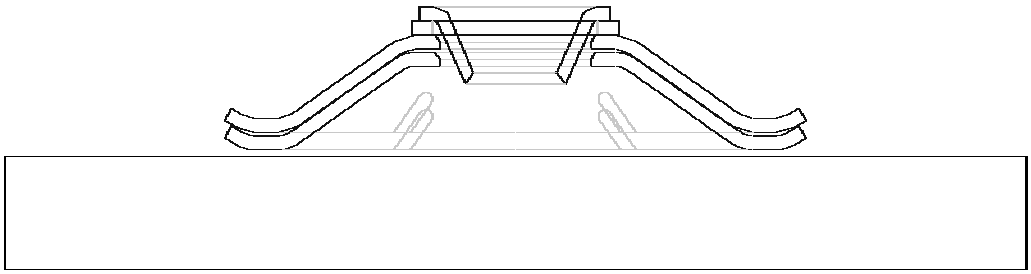

Figure 70 Proposed improvement n°2

3 IMPLEMENTATION OF THE CONNECTION IN A GLOBAL MODEL

Such a study could help define overall force-displacement curves or approximate stiffness value in this type of connection, which could then be implemented in a numerical model of entire structures and thus make their response to seismic actions closer to reality. The design of retrofitting techniques would then be simpler as well as more accurate and efficient in terms of life safety and cultural and economical losses. These numerical models, capable of predicting damage regarding a possible future earthquake and thus estimating losses, are of fundamental importance in seismic vulnerability assessment.

This was not able to be carried out in this particular study because the behaviour of the plate was not satisfying and the operation too time consuming. It could perhaps be proposed as a topic for another master thesis.

A possible solution could be the implementation of such a response in a numerical model of an entire structure done by means of interface elements to which a non linear behaviour, describing the connection response, would be attached. The force-displacement diagram could be reproduced through the stress-strain diagram of the interface element and a calibration of the element regarding the real response of the plate could make the simple model accurate.

CHAPTER 8: CONCLUSIONS

1. CONCLUSIONS

An experimental campaign was carried out in the structural laboratory of the University of Minho in order to have a first idea of the seismic behaviour of the ductile plate. It was observed that the prototype is characterized by an ultimate load of 95kN reached by means of a stiffness of 55kN/m which undergoes degradation during the cyclic loading. It was also noticed that for each of the cycles the plate was did not recover its initial shape once in the plastic range. Moreover, each cycle was described by a small loop on the force – displacement diagram corresponding to a dissipation of energy through friction and plasticization of the material.

Based on these experiments, a numerical model developed previously was calibrated and analysed. A numerical parametric study was carried out in order to determine the properties of the steel. Finally, a comparison of the experimental results with the numerical ones led to a discussion on the seismic response of the connection. It was confirmed that the plate did not reach expectations in terms of seismic behaviour because of the residual displacement and the small amount of energy dissipated through the cycles.

Finally, the prototype was compared with the structural elements connected to the plate once implemented on a building. It was shown that both the stiffness of the connected element and their ultimate load were an important factor in the design process of a ductile connection. Consequently, the element of the connection expected to deform and dissipate energy, in this case the anchor plate, should be the weakest part of the connection. It was also concluded that a ductile connection should behave in a flag shaped hysteresis way, which is not the case of this anchor plate.

2. RECOMMENDATIONS

From the study carried out in this thesis, several recommendations are pointed out in order to advise the future potential user of various issues.

First of all, it was recommended to implement the plate on a rigid plate fixed to the wall by means of resins for example. It was observed during both the numerical and experimental campaign that from the moment the plate started to deform, the support conditions changed from a line to punctual supports which could lead to the masonry being crushed and thus damage the historical material.

Another recommendation would be to carefully select the tie rod to be fixed to the plate according to its stiffness. As explained previously, the plate has to be the weakest element of the structural system in order to have greater deformation and thus dissipate energy. Furthermore, attention should be paid

to the stiffness of the wall, and if the latter is too weak, seismic retrofitting techniques should be implemented in order to reinforce the wall itself in addition to the ductility added by the plate.

Finally, a warning would be given on the implementation of this plate on seismic areas with high PGAs. If the ultimate load of the plate is reached, the anchor would deform inelastically and thus not recover its initial position. In this way, the confinement of the structural element, such as perpendicular and parallel walls, due to the tie-rod would not be efficient anymore. In addition to the absence of confinement of the walls, the squeezed plate, together with steel ties, could add a non expected dynamic effect to the system and thus increase the seismic vulnerability of the building. For these reasons, great care should be taken by choosing to implement this connection.

3. FURTHER WORK

It has been observed throughout this study that the plate was not reaching expectations in terms of energy dissipation and seismic behaviour. Therefore, it would be advisable to think of possible improvements to be made to the plate in order to improve its seismic response. As an adviser, attention should be paid to the frictional phenomenon analysed as the most efficient one to dissipate energy. One of the main issues of the plate was observed to be the residual deformations once the anchor was squeezed. In this way, the other problem to be addressed would be to recover the initial shape by, for example, means of improving the steel characteristics in order to obtain a flag shaped hysteresis. Moreover, if the static analysis of the improved plate led to interesting results, the dynamic effect should be also studied in order to be closer to a real excitation.

Furthermore, a system not presented in this work, made out of two plates linked to an arm connected to the steel tie, was developed and could be studied more deeply. Of course, the whole system is interesting but the plate should be improved or replaced by another dissipative system. As explained in the last chapter of this thesis, this structural ductile system will be governed by the different stiffness of the elements constituting the connection. Thus, attention should be paid in order to have a beam defined with a stiffness in the same range as a stiffness equivalent to two anchors.

Finally, research in the field of efficient connection in historical buildings needs to be developed and improvement in the structure’s ductility is to be taken into consideration. In the scope of seismic retrofitting, new prototypes could be designed such as the one presented in this thesis in order to allow our cultural heritage to undergo a seismic event without suffering important damage. Should an efficient system be developed, it would be of great interest to define its structural characteristics in order to be able to implement the ductile system in a simple way in a global model and thus be able to predict a seismic response of a building more accurately.

REFERENCES

[1] M. Riuscetti, R. Carniel, and C. Cecotti, “Seismic vulnerability assessment of masonry buildings in a region of moderate seismicity,” *Annali di geofisica*, vol. XL, no. 5, p. 9, 1997.

[2] EU-India Economic Cross Cultural Programme, “Guidelines for the conservation of historical masonry structures in seismic areas,” 2006.

[3] H. Sandi, A. Pomonis, S. Francis, and E. Georgescu, “Seismic vulnerability assessment: Methodological elements and applications to the case of Romania,” *Munich Personal RePEc Archive*, no. 25724, 2007.

[4] G. M. Calvi, R. Pinho, G. Magenes, J. J. Bommer, and H. Crowley, “Development of seismic vulnerability assessment methodologies over the past 30 years,” *Journal of Earthquake Technology*, vol. 43, no. 472, pp. 75-104, 2006.

[5] A. Menon and G. Magenes, “Definition of Seismic Input for Out-of-Plane Response of Masonry Walls: I. Parametric Study,” *Journal of Earthquake Engineering*, vol. 15, no. 2, pp. 165-194, Jan. 2011.

[6] L. F. Ramos and P. B. Lourenço, “Modeling and vulnerability of historical city centers in seismic areas: a case study in Lisbon,” *Engineering Structures*, vol. 26, no. 9, pp. 1295-1310, Jul. 2004.

[7] M. R. Valluzzi and C. Modena, “Mechanical behaviour of masonry structures strengthened with different improvement techniques,” pp. 137-156, 2006.

[8] EU-India Economic Cross Cultural Programme, “Identification of strenghtenning strategies,” 2006.

[9] Federal Emergency Management Agency, “NEHRP guidelines for the seismic rehabilitation of buildings - FEMA 273,” 1997.

[10] T.-J. Lin and J. M. LaFave, “Experimental structural behavior of wall-diaphragm connections for older masonry buildings,” *Construction and Building Materials*, vol. 26, no. 1, pp. 180-189, Jan. 2012.

[11] B. W. B. Cross and N. P. Jones, “Seismic performance of joist-pocket connections: I.Modeling,” vol. 119, no. 10, pp. 2986-3007, 1994.

[12] M. Tomazevic, *Earthquake-resistant design of masonry buildings*, Imperial C. 1999, p. 268.

[13] M. Tomazevic, M. Lutman, and P. Weiss, “Seismic upgrading of old brick-masonry urban houses: tying of walls with steel ties,” *Earthquake spectra*, vol. 12, no. 3, pp. 599-622, 1996.

[14] A. Plumier, “Behaviour of Connections,” vol. 29, pp. 95-119, 1994.

[15] Solid Works, “Understanding Nonlinear Analysis,” 2008.

[16] P. B. Lourenço, *Métodos computacionais na mecânica dos sólidos não-linear*. 1999, p. 124.

[17] M. Jirásek and P. B. Lourenço, “Classes presentation from Msc SAHC,” 2012.

[18] A. Kossa and L. Szabó, “Exact integration of the von Mises elastoplasticity model with combined linear isotropic-kinematic hardening,” *International Journal of Plasticity*, vol. 25, no. 6, pp. 1083-1106, 2009.

[19] N. Nemati, D. Le Houedec, and R. Zandonini, “Numerical modelling of the cyclic behaviour of the basic components of steel end plate connections,” *Advances in Engineering Software*, vol. 31, no. 11, pp. 837-849, Nov. 2000.

[20] C. Castiglioni, L. Calado, A. Plumier, P. Thanopoulos, and I. Vayas, “Behaviour of seismic resistant braced frames with innovative dissipative (INERD) connections,” 2004.

[21] L. Guerreiro, “Sistemas de Protecção Sísmica de Estruturas,” pp. 1-53, 2007.

[22] M. Newcombe, “Seismic design of multistorey post-tensioned timber buildings,” 2007.

[23] A. Palermo, S. Pampanin, A. Buchanan, and M. Newcombe, “Seismic Design of Multi-Storey Buildings using Laminated Veneer Lumber (LVL),” *2005 NZSEE Conference, Wairaki, New Zealand*, p. 8, 2005.

[24] M. J. N. Priestley, “Overview of PRESSS Research Program,” *PCI journal*, vol. 36(4), pp. 50-57, 1991.

[25] M. J. N. Priestley, S. Sritharan, J. R. Conley, and S. Pampanin, “Preliminary Results and Conclusions from the PRESSS Five-story Precast Concrete Test-Building,” *PCI journal*, vol. 44(6), pp. 42-67, 1999.

[26] M. J. N. Priestley and J. R. Tao, “Seismic Response of Precast Prestressed Concrete Frames With Partially Bonded Tendons,” *PCI journal*, pp. 58-67, 1993.

[27] P. Franchetti, “Classes presentation from Msc SAHC,” 2012.

[28] NIKER, “NIKER,” 2009. [Online]. Available: http://www.niker.eu/.

[29] TNO Building Construction and Research, “Diana Finite Element Analysis User’s manuals, Version 9.3, The Netherlands.” 2008.

[30] I. Aerospace Specification Metals, “ASM.” [Online]. Available: http://asm.matweb.com.

[31] T. M. H. Luong, “Identification of the tensile force in tie-rods using modal analysis tests.,” 2010.

ANNEX 1: SPECIMENS DIMENSIONS SUMMARY

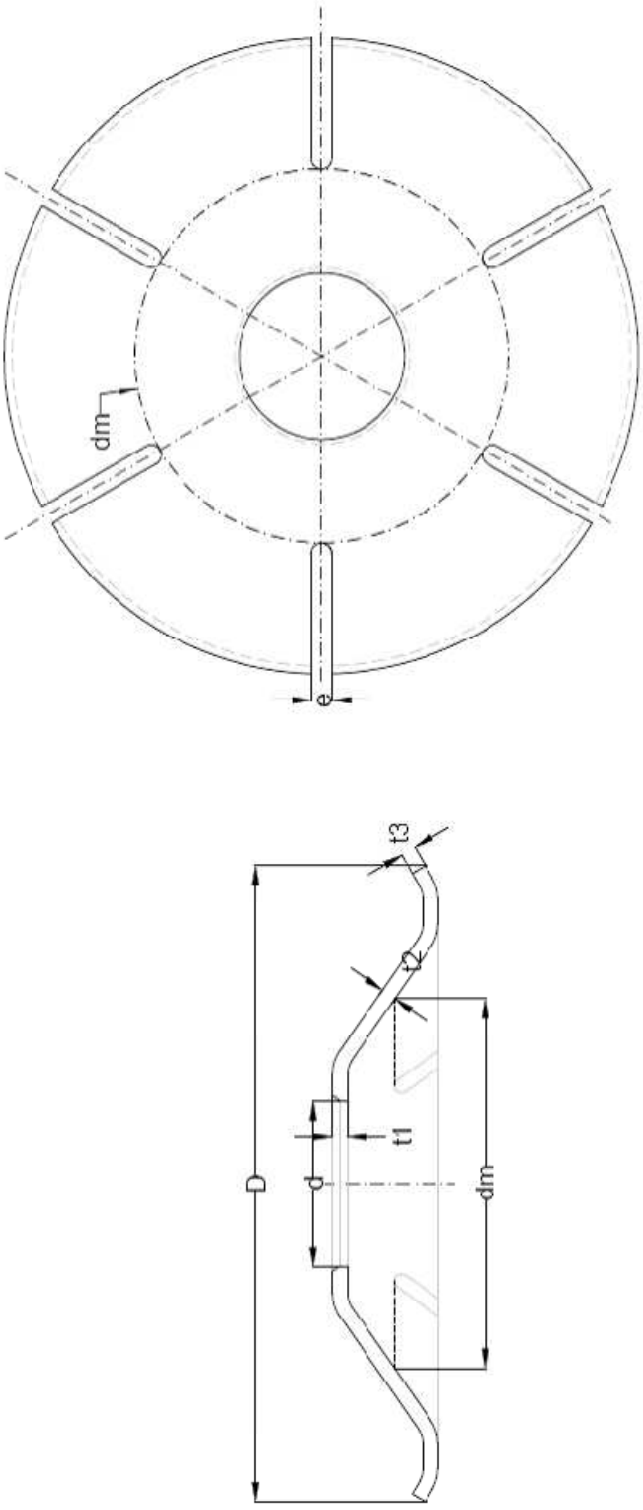

Figure 71 location of measured dimensions

Plates		DP 1	DP 1 Average	DP 2	DP 2 Average	DP 3	DP 3 Average	DP 4	DP 4 Average	DP 5	DP 5 Average	DP 6	DP 6 Average	DP 7	DP 7 Average
Diameters	D (mm)	255,84	256,07	256,09	256,16	255,87	256,03	256,34	256,19	256,14	256,23	255,75	256,11	256,31	256,22
		255,93		256,10		256,40		255,89		256,34		256,24		256,12	
		256,44		256,30		255,83		256,33		256,20		256,35		256,24	
	dm (mm)	147,82	147,49	147,14	147,27	147,34	147,49	147,43	147,56	147,58	147,40	147,30	147,22	147,09	147,16
		147,25		147,12		147,51		147,46		147,27		147,16		147,17	
		147,39		147,56		147,61		147,78		147,36		147,20		147,22	
	d (mm)	65,30	65,25	65,48	65,46	65,23	65,22	65,74	65,73	65,75	65,75	65,00	65,17	65,40	65,21
		65,26		65,45		65,20		65,72		65,74		65,20		65,33	
		65,18		65,45		65,22		65,72		65,75		65,31		64,91	
Thicknesses	t1 (mm)	6,11	6,12	5,85	5,84	5,95	5,96	5,79	5,86	5,96	6,03	5,78	5,75	5,70	5,74
		6,17		5,88		5,76		6,08		6,08		5,75		5,76	
		6,09		5,79		6,16		5,71		6,04		5,71		5,77	
	t2 (mm)	5,98	5,92	6,02	5,97	5,91	5,87	5,86	5,95	5,93	5,99	5,82	5,87	5,92	5,96
		5,89		5,98		5,85		6,02		6,08		5,95		5,95	
		5,90		5,91		5,85		5,96		5,96		5,85		6,00	
	t3 (mm)	6,09	6,08	6,07	5,98	5,97	6,03	6,18	6,10	6,01	6,02	6,02	6,11	6,10	6,15
		6,09		5,93		5,94		6,08		5,98		6,18		6,21	
		6,06		5,94		6,17		6,05		6,08		6,12		6,14	
Heights	h1 (mm)	41,00	40,83	41,00	41,00	41,00	40,83	41,50	41,17	42,00	41,67	42,00	41,50	42,00	41,67
		40,50		41,00		40,50		41,00		41,50		41,00		41,00	
		41,00		41,00		41,00		41,00		41,50		41,50		42,00	
	h2 (mm)	22,00	22,33	23,00	22,00	23,00	23,00	22,00	21,83	22,00	22,83	23,00	23,67	22,00	22,67
		22,00		21,00		23,00		21,00		23,00		24,00		23,00	
		23,00		22,00		23,00		22,50		23,50		24,00		23,00	
	h3 (mm)	11,00	11,33	11,00	11,17	11,00	11,00	12,00	11,33	11,50	11,50	11,50	11,50	10,50	11,00
		12,00		11,50		11,50		11,00		11,00		11,00		11,50	
		11,00		11,00		10,50		11,00		12,00		12,00		11,00	
Openings widths (mm)	e1	7,98	8,08	7,87	7,89	8,08	8,11	7,69	7,72	7,70	7,81	8,10	8,04	7,96	8,10
	e2	8,24		7,97		8,16		7,61		7,84		8,00		7,98	
	e3	8,01		7,94		8,24		7,68		7,91		8,08		8,18	
	e4	8,18		7,92		8,09		7,64		7,91		8,07		8,15	
	e5	7,97		7,77		8,05		7,82		7,70		7,93		7,93	
	e6	8,07		7,86		8,03		7,88		7,77		8,08		8,38	

Figure 72 Summary of specimens dimensions (DP1 to DP7)

Plates		DP 8	DP 8 Average	DP 9	DP 9 Average	DP 10	DP 10 Average	DP 11	DP 11 Average	DP 12	DP 12 Average	Averages	Drawing	Error
Diameters	D (mm)	256,21	256,17	256,71	256,19	255,93	256,28	256,60	256,41	256,13	256,14	256,18	250,00	0,02
		256,21		255,80		256,58		256,62		256,32				
		256,09		256,06		256,34		256,01		255,97				
	dm (mm)	146,94	147,08	147,06	147,31	147,20	147,38	146,98	147,03	147,93	148,05	147,37	147,00	0,00
		146,98		147,37		147,62		147,06		147,84				
		147,32		147,49		147,32		147,05		148,37				
	d (mm)	65,38	65,36	65,33	65,01	65,40	65,39	65,82	65,74	65,87	65,86	65,43	65,00	0,01
		65,39		64,49		65,38		65,62		65,85				
		65,31		65,22		65,39		65,77		65,86				
Thicknesses	t1 (mm)	5,60	5,59	5,57	5,68	5,68	5,74	6,04	6,01	5,98	5,90	5,85	6,00	0,02
		5,58		5,65		5,84		6,03		6,08				
		5,58		5,82		5,70		5,96		5,65				
	t2 (mm)	5,85	5,76	5,83	5,82	5,85	5,86	6,01	5,95	5,66	5,66	5,88	6,00	0,02
		5,74		5,81		5,82		5,91		5,68				
		5,70		5,82		5,91		5,93		5,63				
	t3 (mm)	5,86	5,96	5,87	5,97	6,06	5,99	6,03	6,13	5,84	5,87	6,03	6,00	0,01
		6,04		5,89		5,96		6,23		5,92				
		5,97		6,15		5,95		6,14		5,86				
Heights	h1 (mm)	42,00	41,67	41,00	41,17	41,00	41,33	41,50	41,50	41,50	41,67	41,33	41,50	0,00
		41,50		42,00		41,00		41,50		41,50				
		41,50		40,50		42,00		41,50		42,00				
	h2 (mm)	23,00	23,00	23,00	22,67	23,00	22,83	23,00	22,83	23,00	23,33	22,75	-	-
		23,00		22,50		23,50		22,50		23,00				
		23,00		22,50		22,00		23,00		24,00				
	h3 (mm)	11,00	11,00	11;5	11,50	11,00	11,17	11,00	11,17	11,50	11,50	11,26	11,00	0,02
		11,00		12,00		11,50		11,00		12,00				
		11,00		11,00		11,00		11,50		11,00				
Openningss widths (mm)	e1	8,01	8,06	8,14	8,02	7,92	8,05	7,95	7,98	7,92	8,04	7,99	8,00	0,00
	e2	8,13		8,00		7,94		7,98		8,08				
	e3	7,97		8,11		8,10		7,94		8,07				
	e4	8,08		8,16		7,98		7,97		8,03				
	e5	8,02		7,79		8,20		8,03		8,07				
	e6	8,16		7,92		8,14		7,99		8,05				

Figure 73 Sumary of specimens dimensions (DP8 to DP12)

ANNEX 2: CYCLIC TEST PROCEDURE

rate	Δt (s)	Time (s)	d (mm)	Hours
0		0	0,00	0,00
-0,01	125	125	-1,25	0,03
0,01	75	200	-0,50	0,06
-0,01	75	275	-1,25	0,08
0,01	75	350	-0,50	0,10
-0,01	200	550	-2,50	0,15
0,01	200	750	-0,50	0,21
-0,01	200	950	-2,50	0,26
0,01	200	1150	-0,50	0,32
-0,01	325	1475	-3,75	0,41
0,01	225	1700	-1,50	0,47
-0,025	90	1790	-3,75	0,50
0,025	90	1880	-1,50	0,52
-0,025	140	2020	-5,00	0,56
0,025	96	2116	-2,60	0,59
-0,025	96	2212	-5,00	0,61
0,025	96	2308	-2,60	0,64
-0,05	80	2388	-6,60	0,66
0,05	52	2440	-4,00	0,68
-0,05	52	2492	-6,60	0,69
0,05	52	2544	-4,00	0,71
-0,05	86	2630	-8,30	0,73
0,05	52	2682	-5,70	0,75
-0,05	52	2734	-8,30	0,76
0,05	52	2786	-5,70	0,77
-0,05	86	2872	-10,00	0,80
0,05	52	2924	-7,40	0,81
-0,05	52	2976	-10,00	0,83
0,05	52	3028	-7,40	0,84
-0,05	102	3130	-12,50	0,87
0,1	28	3158	-9,70	0,88
-0,05	56	3214	-12,50	0,89
0,1	28	3242	-9,70	0,90
-0,05	106	3348	-15,00	0,93
0,1	30	3378	-12,00	0,94
-0,05	60	3438	-15,00	0,96
0,1	30	3468	-12,00	0,96
-0,05	160	3628	-20,00	1,01
0,1	30	3658	-17,00	1,02
-0,05	60	3718	-20,00	1,03
0,1	200	3918	0,00	1,09

Figure 74 History of the cyclic loading procedure

ANNEX 3: STIFFNESS DEGRADATION

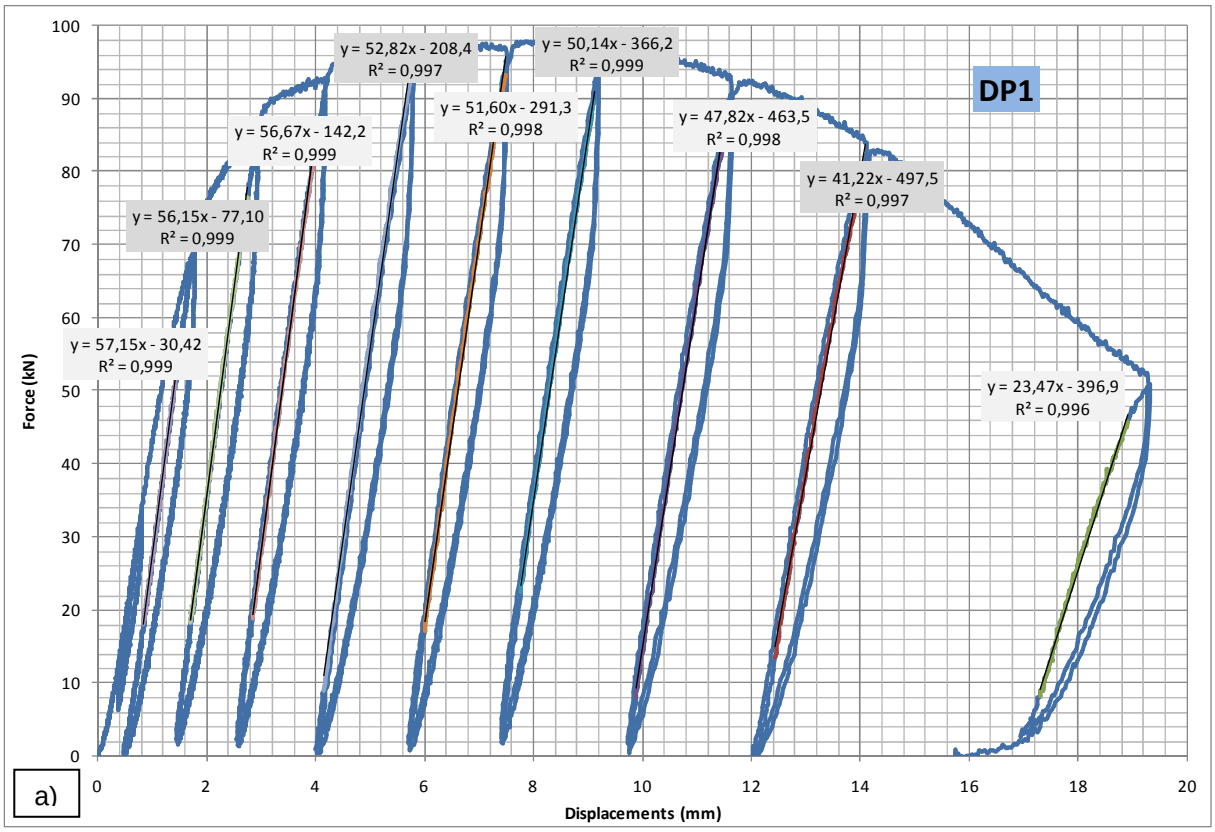

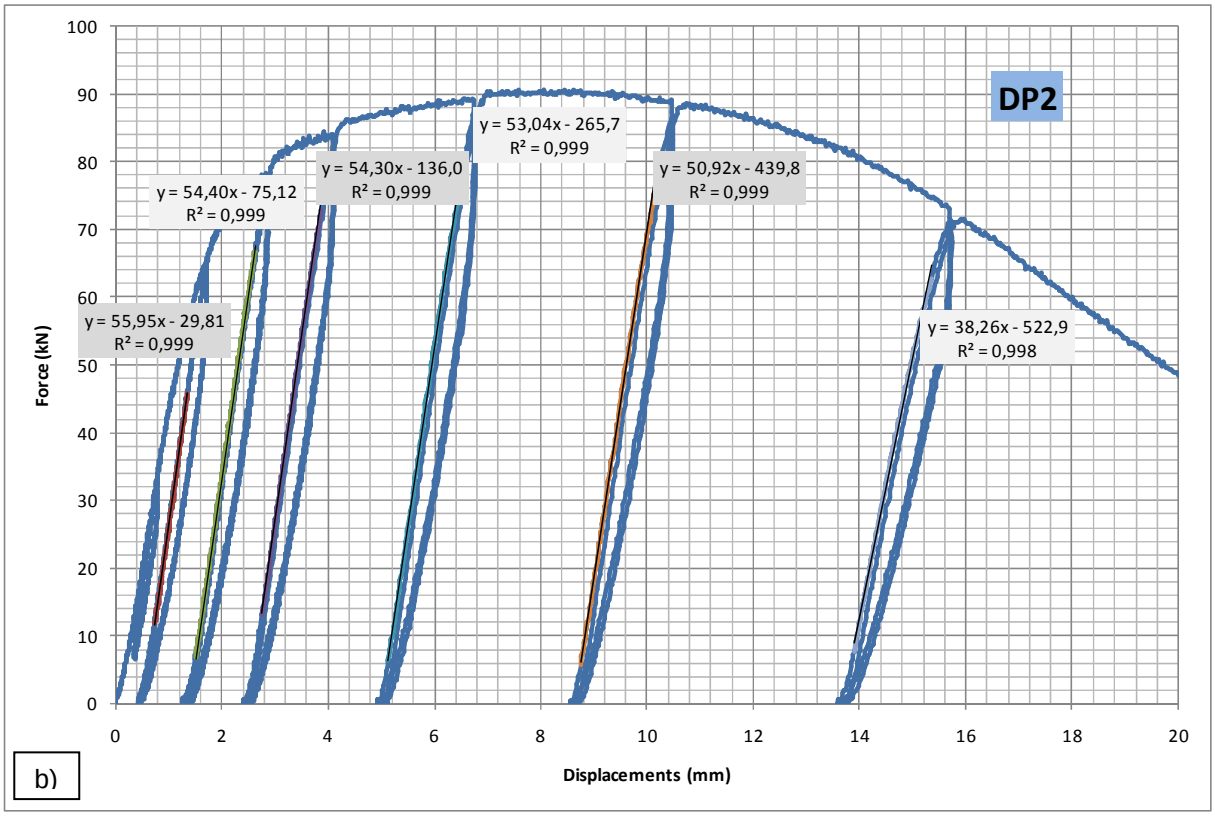

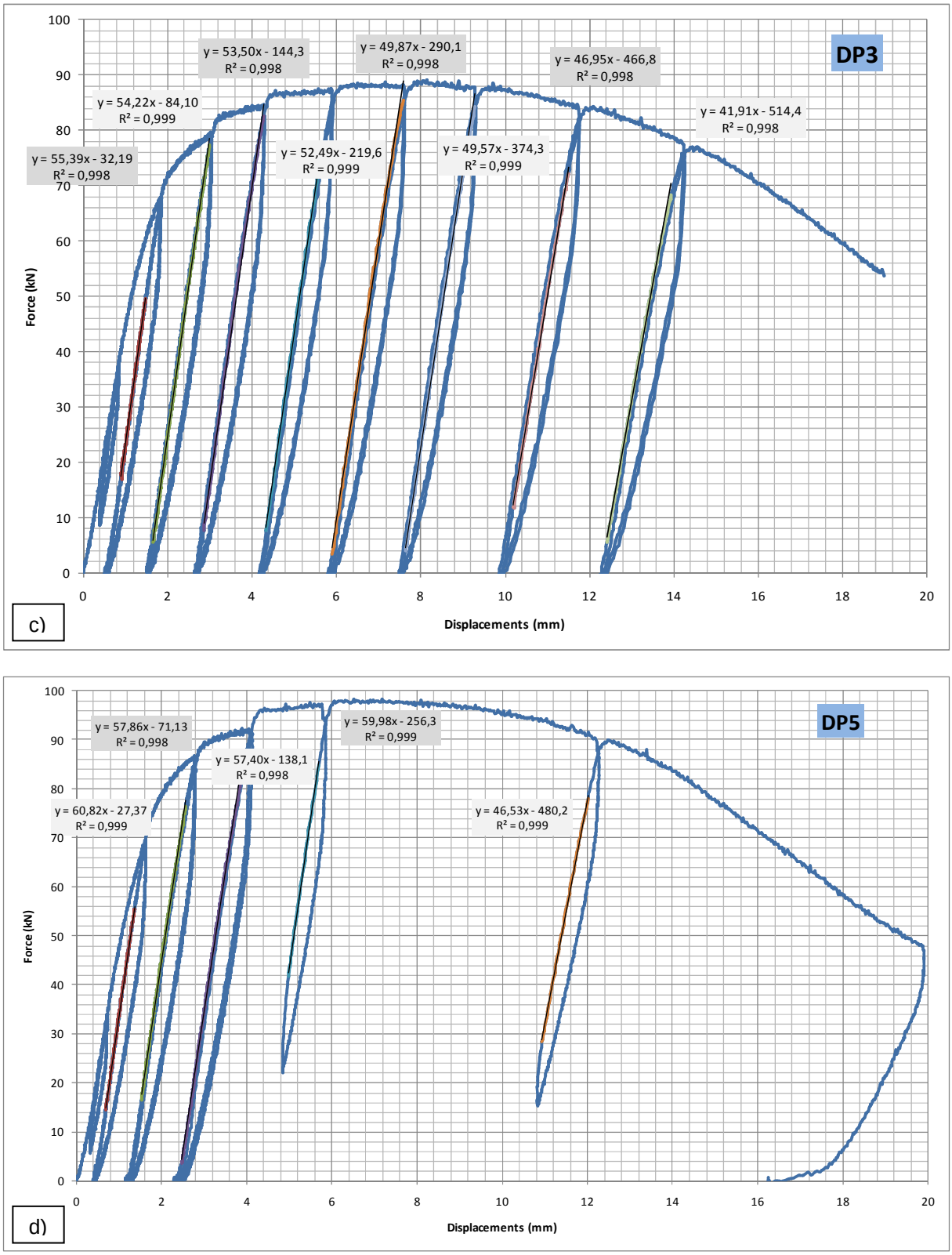

Figure 75 Cyclic response of the specimens with stiffness degradation a)DP1 b)DP2 c)DP3 d)DP5